

Rethinking Link Prediction for Directed Graphs

Mingguo He¹ Yuhe Guo¹ Yanping Zheng¹ Zhewei Wei¹ Stephan Günnemann² Xiaokui Xiao³

Abstract

Link prediction for directed graphs is a crucial task with diverse real-world applications. Recent advances in embedding methods and Graph Neural Networks (GNNs) have shown promising improvements. However, these methods often lack a thorough analysis of embedding expressiveness and suffer from ineffective benchmarks for a fair evaluation. In this paper, we propose a unified framework to assess the expressiveness of existing methods, highlighting the impact of dual embeddings and decoder design on performance. To address limitations in current experimental setups, we introduce **DirLinkBench**, a robust new benchmark with comprehensive coverage and standardized evaluation. The results show that current methods struggle to achieve strong performance on the new benchmark, while DiGAE outperforms others overall. We further revisit DiGAE theoretically, showing its graph convolution aligns with GCN on an undirected bipartite graph. Inspired by these insights, we propose a novel spectral directed graph auto-encoder **SDGAE** that achieves SOTA results on DirLinkBench. Finally, we analyze key factors influencing directed link prediction and highlight open challenges. The code is available at [here](#).

1. Introduction

A directed graph (or digraph) is a type of graph in which the edges between nodes have a specific direction. These graphs are often used to model real-world asymmetric relationships, such as “following” and “followed” in social networks (Leskovec & Sosič, 2016) or “link” and “linked” in web pages (Page et al., 1999). Directed graphs reflect the inherent directionality of relationships and provide a more accurate representation of complex systems. Link prediction is a critical and common task for directed graphs with diverse real-world applications. Examples include

¹Gaoling School of Artificial Intelligence, Renmin University of China ²Technical University of Munich ³National University of Singapore. Contact to: Mingguo He <mingguo@ruc.edu.cn>.

Table 1. Overview of directed graph learning methods.

Method	Name	Embedding
Embedding Methods	HOPE (Ou et al., 2016)	s_u, t_u
	APP (Zhou et al., 2017)	s_u, t_u
	AROPE (Zhang et al., 2018)	s_u, t_u
	STRAP (Yin & Wei, 2019)	s_u, t_u
	NERD (Khosla et al., 2020)	s_u, t_u
	DGGAN (Zhu et al., 2021)	s_u, t_u
	ELTRA (Hamedani et al., 2023)	s_u, t_u
Graph Neural Networks	ODIN (Yoo et al., 2023)	s_u, t_u
	DiGAE (Kollias et al., 2022)	s_u, t_u
	CoBA (Liu et al., 2023)	s_u, t_u
	BLADE (Virinchi & Saladi, 2023)	s_u, t_u
	Gravity GAE (Salha et al., 2019)	h_u, m_u
	DHYPR (Zhou et al., 2022)	h_u, m_u
	DGCN (Tong et al., 2020b)	h_u
	DiGCN & DiGCNIB (Tong et al., 2020a)	h_u
	DirGNN (Rossi et al., 2024)	h_u
	HoloNets (Koke & Cremers, 2024)	h_u
	NDDGNN (Huang et al., 2024)	h_u
	MagNet (Zhang et al., 2021)	z_u
	LightDiC (Li et al., 2024)	z_u
	DUPLEX (Ke et al., 2024)	z_u

predicting follower relationships in social networks (Liben-Nowell & Kleinberg, 2003), recommending products in e-commerce (Rendle et al., 2009), and detecting intrusions in network security (Bhuyan et al., 2013).

Machine learning techniques have been extensively developed to enhance link prediction performance on directed graphs. Existing methods can be broadly categorized into **embedding methods** and **graph neural networks (GNNs)**. Embedding methods aim to preserve the asymmetry of directed graphs by generating two separate embeddings for each node u : a source embedding s_u and a target embedding t_u (Hamedani et al., 2023; Yoo et al., 2023), which are also known as content/context representations (Ou et al., 2016; Yin & Wei, 2019). GNNs, on the other hand, can be further divided into four classes based on the types of embeddings they generate. (1) Source-target methods, similar to embedding methods, employ specialized propagation mechanisms to learn distinct source and target embeddings for each node (Kollias et al., 2022; Liu et al., 2023). (2) Gravity-inspired methods, inspired by Newton’s law of universal gravitation, learn a real-valued embedding $h_u \in \mathbb{R}^d$ and a mass parameter $m_u \in \mathbb{R}^+$ for each node u (Salha et al., 2019; Zhou et al., 2022). (3) Single real-valued methods follow a conventional approach by learning a single

Table 2. A unified framework for directed link prediction methods, with detailed descriptions provided in Appendix D.

Encoder $\text{Enc}(\cdot)$	Embeddings (θ_u, ϕ_u)	Possible Decoder $\text{Dec}(\cdot)$
Source-target	$s_u = \theta_u, \quad t_u = \phi_u$	$\sigma(s_u^\top t_v); \quad \text{LR}(s_u \odot t_v); \quad \text{LR}(s_u \ t_v)$
Single real-valued	$h_u = \theta_u, \quad \phi_u = \phi_u$	$\sigma(h_u^\top h_v); \quad \text{MLP}(h_u \odot h_v); \quad \text{MLP}(h_u \ h_v)$
Complex-valued	$z_u = \theta_u \odot \exp(i\phi_u)$	$\text{Direc}(z_u, z_v); \quad \text{MLP}(\theta_u \ \theta_v \ \phi_u \ \phi_v)$
Gravity-inspired	$h_u = \theta_u, \quad m_u = g(\phi_u)$	$\sigma(m_v - \lambda \log \ h_u - h_v\ _2^2); \quad \sigma(m_v - \lambda \log(\text{dist}_{\mathbb{D}_c^{d'}}(h_u, h_v)))$

real-valued embedding $h_u \in \mathbb{R}^d$ (Rossi et al., 2024; Huang et al., 2024). (4) Complex-valued methods use Hermitian adjacency matrices, learning complex-valued embeddings $z_u \in \mathbb{C}^d$ (Zhang et al., 2021; Ke et al., 2024). We summarize these methods in Table 1.

Although the methods described above have achieved promising results in directed link prediction, several challenges remain. First, it is unclear what types of embedding are effective in predicting directed links, as there is a lack of comprehensive research assessing these methods’ expressiveness. Second, existing methods have not been fairly compared and evaluated, highlighting the need for a robust benchmark for directed link prediction. Current experimental setups face multiple issues, such as the omission of basic baselines (e.g. MLP shown in Figures 1(a) and 1(b)), label leakage (illustrated in Table 3), class imbalance (Figure 1(c)), single evaluation metrics, and inconsistent dataset splits. We discuss these issues in detail in Section 2.2.

In this paper, we first propose a unified learning framework for directed link prediction methods to assess the expressiveness of different embedding types. We show that dual embeddings, encompassing all existing types except single real-valued ones, are critical for effective directed link prediction. Meanwhile, we highlight the often-overlooked importance of decoder design in achieving better performance, as most research has primarily focused on encoders. To address the limitations of existing experimental setups, we present **DirLinkBench**, a robust new directed link prediction benchmark with comprehensive coverage (7 datasets, 15 baselines), standardized evaluation (unified splits, features, and tasks), and modular extensibility (supporting new datasets, decoders, and sampling strategies).

The results in DirLinkBench reveal that current methods struggle to achieve strong and firm performance across diverse datasets. Notably, a simple directed graph auto-encoder, DiGAE (Kollias et al., 2022), outperforms others in general. We revisit DiGAE from a theoretical perspective and observe that its graph convolution is equivalent to the GCN (Kipf & Welling, 2017) convolution on an undirected bipartite graph. Building on this insight, we propose **SDGAE**, a novel directed graph auto-encoder that learns propagation weights via spectral-based GNN (Chien et al.,

2021) techniques. SDGAE achieves state-of-the-art results on four of the seven datasets and ranks highest on average. Finally, we investigate key factors influencing directed link prediction (e.g., input features, decoder design, and degree distribution) and conclude with open challenges to advance the field. We summarize our contributions as follows.

- We propose a unified framework to assess the expressiveness of directed link prediction methods, showing that dual embeddings and suitable decoders are critical.
- We introduce DirLinkBench, a robust new benchmark with comprehensive coverage and standardized evaluation for directed link prediction tasks.
- We propose a novel directed graph auto-encoder SDGAE, inspired by the theoretical insights of DiGAE and achieving state-of-the-art results on DirLinkBench.
- We empirically analyze the factors affecting the performance of directed link prediction and highlight open challenges for future research.

2. Rethinking Directed Link Prediction

In this section, we will first revisit the link prediction task for directed graphs and introduce a unified framework to assess the expressiveness of existing methods. Next, we examine the current experimental setups for directed link prediction and highlight several associated issues.

Notation. We consider a directed, unweighted graph $\mathcal{G} = (V, E)$, with node set V and edge set E . Let $n = |V|$ and $m = |E|$ represent the number of nodes and edges in \mathcal{G} , respectively. We use \mathbf{A} to denote the adjacency matrix of \mathcal{G} , where $A_{uv} = 1$ if there exists a directed edge from node u to node v , and $A_{uv} = 0$ otherwise. The Hermitian adjacency matrix of \mathcal{G} is denoted by \mathbf{H} and defined as $\mathbf{H} = \mathbf{A}_s \odot \exp(i\frac{\pi}{2}\Theta)$. Here, $\mathbf{A}_s = \mathbf{A} \cup \mathbf{A}^\top$ is the adjacency matrix of the undirected graph derived from \mathcal{G} , and $\Theta = \mathbf{A} - \mathbf{A}^\top$ is a skew-symmetric matrix. We denote the out-degree and in-degree matrices of \mathbf{A} by $\mathbf{D}_{\text{out}} = \text{diag}(\mathbf{A}\mathbf{1})$ and $\mathbf{D}_{\text{int}} = \text{diag}(\mathbf{A}^\top\mathbf{1})$, respectively, where $\mathbf{1}$ is the all-one vector. Let $\mathbf{X} \in \mathbb{R}^{n \times d'}$ denote the node feature matrix, where each node has a d' -dimensional feature vector. Key notations of this paper are summarized in Appendix A.

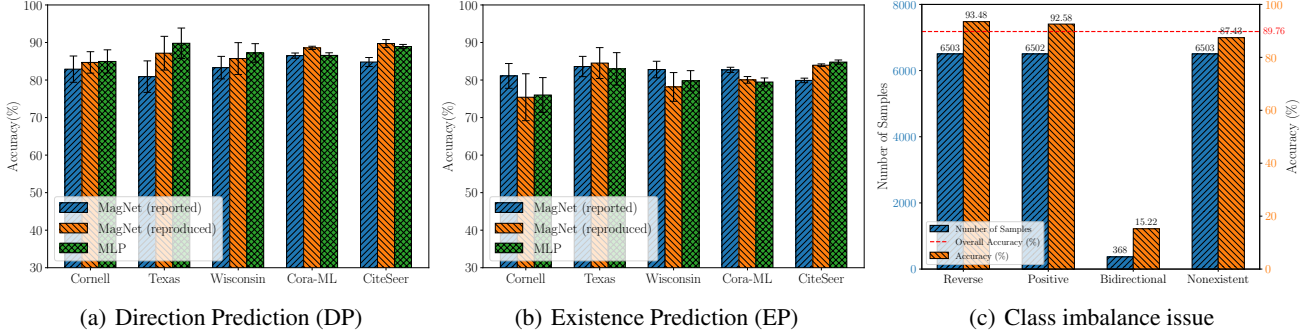


Figure 1. (a) and (b) are the results of MagNet (Zhang et al., 2021) as reported in the original paper, alongside the reproduced MagNet and MLP results. (c) is the number of samples and the accuracy for each class of DUPLEX (Ke et al., 2024) on the Cora dataset in the 4C task.

2.1. Unified Framework for Directed Link Prediction

The link prediction task on directed graphs is to predict potential directed links (edges) in an observed graph \mathcal{G}' , with the given structure of \mathcal{G}' and node feature \mathbf{X} . Formally,

Definition 2.1. Directed link prediction problem. Given an observed graph $\mathcal{G}' = (V, E')$ and node feature \mathbf{X} , the goal of directed link prediction is to predict the likelihood of a directed edge $(u, v) \in E^*$ existing, where $E^* \subseteq (V \times V) \setminus E'$. The probability of edge (u, v) existing is given by

$$p(u, v) = f(u \rightarrow v \mid \mathcal{G}', \mathbf{X}). \quad (1)$$

The $f(\cdot)$ denotes a prediction model, such as embedding methods or GNNs. Unlike link prediction on undirected graphs (Zhang & Chen, 2018), for directed graphs, it is necessary to account for directionality. Specifically, $p(u, v)$ and $p(v, u)$ are not equal; they represent the probability of a directed edge existing from node u to node v , and from node v to node u , respectively. To evaluate the expressiveness of existing methods for directed link prediction, we propose a unified framework:

$$(\theta_u, \phi_u) = \text{Enc}(\mathcal{G}', \mathbf{X}, u), \quad \forall u \in V, \quad (2)$$

$$p(u, v) = \text{Dec}(\theta_u, \phi_u, \theta_v, \phi_v), \quad \forall (u, v) \in E^*. \quad (3)$$

Here, $\text{Enc}(\cdot)$ represents an encoder function, which includes various methods described in the Sec. 1. And $\theta_u \in \mathbb{R}^{d_\theta}$, $\phi_u \in \mathbb{R}^{d_\phi}$ are real-valued dual embeddings of dimensions d_θ and d_ϕ , respectively. $\text{Dec}(\cdot)$ is a decoder function tailored to the specific encoder method. This framework unifies existing methods for directed link prediction, as summarized in Table 2. More details are provided in Appendix D. Based on this framework, we have the following theorem.

Theorem 2.2. For the framework defined by Equations (2) and (3), if $d_\theta, d_\phi > 0$ and sufficiently large, there exist embeddings θ_u, ϕ_u and a decoder $\text{Dec}(\cdot)$ that can correctly compute the probability $p(u, v)$ of any directed edge (u, v) in an arbitrary graph. Conversely, if $d_\theta = 0$ or $d_\phi = 0$, no such embeddings or decoders can compute the correct probability of any edges in an arbitrary graph.

The intuition behind the proof of this theorem is that dual embeddings can effectively reconstruct the structure of a graph. For example, in the source-target embeddings, we have $\mathbf{A}_{uv} = \mathbf{s}_u^\top \mathbf{t}_v$, and in the complex-valued method, $\mathbf{H}_{uv} = \mathbf{z}_u \bar{\mathbf{z}}_v$. The full proof can be found in Appendix B.1. Theorem 2.2 demonstrates that dual embeddings are critical for preserving the asymmetry of directed graphs, and that a suitable decoder function is equally important.

Corollary 2.3. With dual embeddings θ_u and ϕ_u , if there is no suitable decoder $\text{Dec}(\cdot)$, the probability $p(u, v)$ of any edge (u, v) cannot be computed correctly. In contrast, even with one single embedding (θ_u or $\phi_u = \emptyset$), a suitable decoder can improve the ability to compute edge probabilities.

The proof is given in Appendix B.2. This corollary shows that dual embeddings require suitable decoders for theoretical expressiveness, while single embeddings, though fundamentally limited, can still benefit from specific decoders in practice. For example, complex-valued methods using $\text{MLP}(\theta_u \parallel \theta_v \parallel \phi_u \parallel \phi_v)$ (Zhang et al., 2021) and single real-valued methods using $\text{MLP}(\mathbf{h}_u \parallel \mathbf{h}_v)$ (He et al., 2023) have equal expressiveness if embedding dimensions are large.

2.2. Issues with Existing Experimental Setup

The existing directed link prediction experimental setups can be broadly categorized into two types. The first is the **multiple subtask setup**, which includes existence prediction (EP), direction prediction (DP), three-type prediction (3C), and four-type prediction (4C). This approach treats directed link prediction as a multi-class classification problem that requires the prediction of positive, inverse, bidirectional, and nonexistent edges. More details are provided in Appendix E.1. This setup is widely adopted by existing methods (Zhang et al., 2021; He et al., 2023; Fiorini et al., 2023; Lin & Gao, 2023; Ke et al., 2024; Li et al., 2024).

The other category is the **non-standardized setting** defined in various papers (Yin & Wei, 2019; Yoo et al., 2023; Zhou et al., 2022; Kollias et al., 2022; Liu et al., 2023). These settings involve different datasets, inconsistent splitting meth-

Table 3. Link prediction results on Cora dataset under the DUPLEX (Ke et al., 2024) setup: results without superscripts are from the DUPLEX paper, [†] indicates reproduction with test set edges in training, and [‡] indicates reproduction without test set edges in training.

Method	EP(ACC)	EP(AUC)	DP(ACC)	DP(AUC)	3C(ACC)	4C(ACC)
MagNet	81.4±0.3	89.4±0.1	88.9±0.4	95.4±0.2	66.8±0.3	63.0±0.3
DUPLEX	93.2±0.1	95.9±0.1	95.9±0.1	97.9±0.2	92.2±0.1	88.4±0.4
DUPLEX [†]	93.49±0.21	95.61±0.20	95.25±0.16	96.34±0.23	92.41±0.21	89.76±0.25
MLP [†]	88.53±0.22	95.46±0.18	95.76±0.21	99.25±0.06	79.97±0.48	78.49±0.26
DUPLEX [‡]	87.43±0.20	91.16±0.24	88.43±0.16	91.74±0.38	84.53±0.34	81.36±0.46
MLP [‡]	84.00±0.29	91.52±0.25	90.83±0.16	96.48±0.28	72.93±0.21	71.51±0.20

ods, and varying evaluation metrics. We discuss the four issues with existing setups below.

Issue 1: The Multi-layer Perceptron (MLP) is a neglected but powerful baseline. Most existing setups do not report MLP performance. We evaluate MLP across three popular multiple subtask setups: MagNet (Zhang et al., 2021), DUPLEX (Ke et al., 2024), and PyGSD (He et al., 2023) covering their different datasets and baselines. Figures 1(a) and 1(b) present the results of our reproduced MagNet experiments alongside the MLP results, showing that MLP performs comparably to MagNet on DP and EP tasks. Table 3 shows the replicated DUPLEX experiments and MLP results on the Cora dataset, demonstrating that MLP achieves competitive performance. Interestingly, while DUPLEX represents the latest advancement in directed graph learning, MLP outperforms it in certain tasks. These findings highlight the absence of basic baselines in prior work and suggest that current benchmarks lack sufficient challenge.

Issue 2: Many benchmarks suffer from label leakage. As defined in Definition 2.1, directed link prediction aims to predict potential edges from observed graphs, with the key principle that test edges must remain hidden during training to avoid label leakage. However, current setups often violate this principle. For example, 1) MagNet, PyGSD, and DUPLEX expose test edges during negative edge sampling in the training process, indirectly revealing the test edges’ presence to the model. 2) LighDiC (Li et al., 2024) uses eigenvectors of the Laplacian matrix of the entire graph as input features, embedding test edge information in the training input. 3) DUPLEX propagates information across the entire graph during training, making the test edges directly visible to the model. To investigate, we experiment with DUPLEX using its original code. As shown in Table 3, DUPLEX[†] (original settings with label leakage) clearly outperforms DUPLEX[‡] (propagation restricted to training edges) due to label leakage. A similar result is observed with MLP: MLP[†] (using in/out degrees from test edges) significantly outperforms MLP[‡] (using only training-edge degrees). These findings underscore that even the leakage of degree information can significantly impact performance.

Issue 3: Multiple subtask setups result in class imbalances and limited evaluation metrics. The multiple subtask setups treat directed link prediction as a multi-class classification problem, causing significant class imbalances that hinder model training. For example, the 4C task in DUPLEX classifies edges into reverse, positive, bidirectional, and nonexistent. However, bidirectional edges are rare in real-world directed graphs, and reverse edges are often arbitrarily assigned, lacking meaningful physical significance. Figure 1(c) highlights the class imbalance and the challenge of predicting bidirectional edges on the Cora dataset. Additionally, these setups rely heavily on accuracy as an evaluation metric, which provides a limited and potentially misleading assessment. Given the nature of link prediction, ranking metrics such as Hits@K and Mean Reciprocal Rank (MRR) are more suitable—a perspective well established in link prediction for undirected graphs (Li et al., 2023).

Issue 4: Lack of standardization in dataset splits and feature inputs. Current settings face inconsistent dataset splits. In multiple subtask setups, edges are typically split into 80% for training, 5% for validation, and 15% for testing. However, class proportions are further manually adjusted for balance, which leads to varying training and testing ratios across different datasets. Non-standardized setups are more confusing, e.g., ELTRA (Hamedani et al., 2023) uses 90% for training, STRAP (Yin & Wei, 2019) uses 50%, and DiGAE (Kollias et al., 2022) uses 85%, making cross-study results difficult to evaluate. Feature input standards are also lacking. Embedding methods often omit node features, while GNNs require them. MagNet and PyGSD use in/out degrees, DUPLEX uses random normal distributions, LightDiC uses original features or Laplacian eigenvectors, and DHYPR (Zhou et al., 2022) uses identity matrices. This inconsistency undermines reproducibility. As shown in Figure 1 and Table 3, reproduced results often deviate significantly, with some better and others worse.

More details and experimental results are provided in Appendix E.2. These issues emphasize the need for a new benchmark for directed link prediction, allowing fair evaluation and providing a foundation for future research.

Table 4. Results of various methods under on the **Hits@100** metric (mean \pm standard error%). Results ranked **first**, **second**, and **third** are highlighted. TO indicates methods that did not finish running within 24 hours, and OOM indicates methods that exceeded memory limits.

Method	Cora-ML	CiteSeer	Photo	Computers	WikiCS	Slashdot	Epinions	Avg. Rank \downarrow
STRAP	79.09 \pm 1.57	69.32 \pm 1.29	69.16\pm1.44	51.87\pm2.07	76.27\pm0.92	31.43 \pm 1.21	58.99\pm0.82	5.14
ODIN	54.85 \pm 2.53	63.95 \pm 2.98	14.13 \pm 1.92	12.98 \pm 1.47	9.83 \pm 0.47	34.17 \pm 1.19	36.91 \pm 0.47	12.71
ELTRA	87.45\pm1.48	84.97 \pm 1.90	20.63 \pm 1.93	14.74 \pm 1.55	9.88 \pm 0.70	33.44 \pm 1.00	41.63 \pm 2.53	8.57
MLP	60.61 \pm 6.64	70.27 \pm 3.40	20.91 \pm 4.18	17.57 \pm 0.85	12.99 \pm 0.68	32.97 \pm 0.51	44.59 \pm 1.62	10.57
GCN	70.15 \pm 3.01	80.36 \pm 3.07	58.77\pm2.96	43.77\pm1.75	38.37 \pm 1.51	33.16 \pm 1.22	46.10 \pm 1.37	5.71
GAT	79.72 \pm 3.07	85.88\pm4.98	58.06 \pm 4.03	40.74 \pm 3.22	40.47 \pm 4.10	30.16 \pm 3.11	43.65 \pm 4.88	5.86
APPNP	86.02 \pm 2.88	83.57 \pm 4.90	47.51 \pm 2.51	32.24 \pm 1.40	20.23 \pm 1.72	31.87 \pm 1.43	41.99 \pm 1.23	8.00
DGCN	63.32 \pm 2.59	68.97 \pm 3.39	51.61 \pm 6.33	39.92 \pm 1.94	25.91 \pm 4.10	TO	TO	10.29
DiGCN	63.21 \pm 5.72	70.95 \pm 4.67	40.17 \pm 2.38	27.51 \pm 1.67	25.31 \pm 1.84	TO	TO	11.29
DiGCNIB	80.57 \pm 3.21	85.32 \pm 3.70	48.26 \pm 3.98	32.44 \pm 1.85	28.28 \pm 2.44	TO	TO	8.43
DirGNN	76.13 \pm 2.85	76.83 \pm 4.24	49.15 \pm 3.62	35.65 \pm 1.30	50.48\pm0.85	41.74\pm1.15	50.10 \pm 2.06	6.00
MagNet	56.54 \pm 2.95	65.32 \pm 3.26	13.89 \pm 0.32	12.85 \pm 0.59	10.81 \pm 0.46	31.98 \pm 1.06	28.01 \pm 1.72	13.14
DUPLEX	69.00 \pm 2.52	73.39 \pm 3.42	17.94 \pm 0.66	17.90 \pm 0.71	8.52 \pm 0.60	18.42 \pm 2.59	16.50 \pm 4.34	12.14
DHYPR	86.81\pm1.60	92.32\pm3.72	20.93 \pm 2.41	TO	TO	OOM/TO	OOM/TO	10.57
DiGAE	82.06 \pm 2.51	83.64 \pm 3.21	55.05 \pm 2.36	41.55 \pm 1.62	29.21 \pm 1.36	41.95\pm0.93	55.14\pm1.96	4.43
SDGAE	90.37\pm1.33	93.69\pm3.68	68.84\pm2.35	53.79\pm1.56	54.67\pm2.50	42.42\pm1.15	55.91\pm1.77	1.43

3. New Benchmark: DirLinkBench

In this section, we introduce a novel robust benchmark for directed link prediction, **DirLinkBench**, offering three principal advantages: 1) Comprehensive coverage, incorporating seven real-world datasets spanning diverse domains and 15 baseline models; 2) Standardized evaluation, establishing a unified framework for dataset splitting, feature initialization, and task settings to ensure fairness and reliability; and 3) Modular extensibility, built on PyG (Fey & Lenssen, 2019) to enable easy integration of new datasets, model architectures, and configurable modules (e.g., feature initialization, decoder types, and negative sampling). We then detail the implementation of DirLinkBench.

Dataset. We select seven publicly available directed graphs from diverse domains. These datasets include two citation networks, Cora-ML (McCallum et al., 2000; Bojchevski & Günnemann, 2018) and CiteSeer (Sen et al., 2008); two co-purchasing networks, Photo and Computers (Shchur et al., 2018); a weblink network, WikiCS (Mernyei & Cangea, 2020); and two social networks, Slashdot (Ordozgoiti et al., 2020) and Epinions (Massa & Avesani, 2005). These directed graphs differ in both size and average degree. Except for Slashdot and Epinions, each dataset includes original node features. We provide the statistical details and additional descriptions in Appendix G.1. To establish standard evaluation conditions for link prediction methods, we preprocess these datasets by eliminating duplicate edges and self-loop links. Following (Gasteiger et al., 2019; Shchur et al., 2018), we also removed isolated nodes and used the largest weakly connected component.

Task setup. We simplify directed link prediction to a binary classification task: the model determines whether a directed edge exists from u to v . Specifically, given a pre-processed directed graph \mathcal{G} , we randomly split 15% of edges for testing, 5% for validation, and use the remaining 80% for training, and ensure that the training graph \mathcal{G}' remains weakly connected (He et al., 2023). For testing and validation, we sample an equal number of negative edges under the full graph \mathcal{G} visible, while for training, only the training graph \mathcal{G}' is visible. To ensure fairness, we generate 10 random splits using fixed seeds, and all models share the same splits. The model learns from the training graphs and feature inputs to compute $p(u, v)$ for test edges. Feature inputs are provided in three forms: original node features, in/out degrees from the training graph \mathcal{G}' (Zhang et al., 2021), or a random normal distribution matrix (Ke et al., 2024).

Baseline. We carefully select 15 state-of-the-art baselines, including three embedding methods: STRAP (Yin & Wei, 2019), ODIN (Yoo et al., 2023), ELTRA (Hamedani et al., 2023); a basic method MLP; three classic undirected GNNs: GCN (Kipf & Welling, 2017), GAT (Veličković et al., 2018), APPNP (Gasteiger et al., 2019); four single real-valued methods: DGCN (Tong et al., 2020b), DiGCN (Tong et al., 2020a), DiGCNIB (Tong et al., 2020a), DirGNN (Rossi et al., 2024); two complex-valued methods: MagNet (Zhang et al., 2021), DUPLEX (Ke et al., 2024); a gravity-inspired method: DHYPR (Zhou et al., 2022); and a source-target GNN: DiGAE (Kollias et al., 2022). We exclude some recent approaches (e.g., CoBA (Liu et al., 2023), BLADE (Virinchi & Saladi, 2023), NDDGNN (Huang et al., 2024)) due to unavailable code.

Baseline Setting. For the baseline implementations, we rely on the authors’ original released code or popular libraries like PyG and the PyTorch Geometric Signed Directed library (He et al., 2023). For methods without released link-prediction code (e.g., GCN, DGCN), we provide various decoders and loss functions, while for methods with available link-prediction code (e.g., MagNet, DiGAE), we strictly follow the reported settings. We tune hyperparameters using grid search, adhering to the configurations specified in each paper. Further details of each method are in Appendix G.1.

Results. We report results on seven metrics—Hits@20, Hits@50, Hits@100, MRR, AUC, AP, and ACC (detailed metric descriptions are provided in Appendix G.2), with complete results for each dataset in Appendix H. Table 4 highlights the Hits@100 results. These results first show that embedding methods retain a strong advantage even without feature inputs. Second, early single real-valued undirected and directed GNNs also perform competitively, while newer directed GNNs (e.g., MagNet, DUPLEX, DHYPR) exhibit weaker performance or scalability issues. This is because complex-based methods have unsuitable loss functions and decoders, while DHYPR’s preprocessing requires $O(Kn^3)$ time and $O(Kn^2)$ space complexity. We provide further analysis in Sec. 5. Notably, DiGAE, a simple directed graph auto-encoder, emerges as the best performer overall, yet it underperforms on certain datasets (e.g., Cora-ML, CiteSeer), leading to a worse average ranking. This observation motivates us to revisit DiGAE’s design and propose new methods to enhance directed link prediction.

4. New Method: SDGAE

In this section, we first revisit the mode structure of DiGAE and analyze its encoder graph convolution. We then propose a novel Spectral Directed Graph Auto-Encoder (SDGAE).

4.1. Understand the Graph Convolution of DiGAE

DiGAE (Kollias et al., 2022) is a graph auto-encoder designed for directed graphs. Its encoder graph convolutional layer is denoted as

$$\mathbf{S}^{(\ell+1)} = \sigma \left(\hat{\mathbf{D}}_{\text{out}}^{-\beta} \hat{\mathbf{A}} \hat{\mathbf{D}}_{\text{in}}^{-\alpha} \mathbf{T}^{(\ell)} \mathbf{W}_T^{(\ell)} \right), \quad (4)$$

$$\mathbf{T}^{(\ell+1)} = \sigma \left(\hat{\mathbf{D}}_{\text{in}}^{-\alpha} \hat{\mathbf{A}}^\top \hat{\mathbf{D}}_{\text{out}}^{-\beta} \mathbf{S}^{(\ell)} \mathbf{W}_S^{(\ell)} \right). \quad (5)$$

Here, $\hat{\mathbf{A}} = \mathbf{A} + \mathbf{I}$ denotes the adjacency matrix with added self-loops, and $\hat{\mathbf{D}}_{\text{out}}$ and $\hat{\mathbf{D}}_{\text{in}}$ represent the corresponding out-degree and in-degree matrices, respectively. $\mathbf{S}^{(\ell)}$ and $\mathbf{T}^{(\ell)}$ denote the source and target embeddings at the ℓ -th layer, initialized as $\mathbf{S}^{(0)} = \mathbf{T}^{(0)} = \mathbf{X}$. The hyperparameters α and β are degree-based normalization factors, σ is the activation function (e.g., ReLU), and $\mathbf{W}_T^{(\ell)}, \mathbf{W}_S^{(\ell)}$ represents the learnable weight matrices.

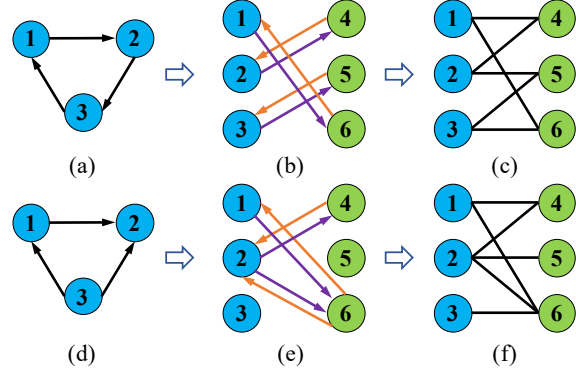


Figure 2. The bipartite representations of two toy directed graphs.

The design of this graph convolution is inspired by the connection between GCN (Kipf & Welling, 2017) and the 1-WL (Weisfeiler & Leman, 1968) algorithm for directed graphs. However, the underlying principles of this convolution remain unexplored, leaving its meaning unclear. Additionally, the heuristic hyperparameters α and β introduce significant challenges for parameter optimization.

We revisit the graph convolution of DiGAE and observe it corresponds to the GCN convolution (Kipf & Welling, 2017) applied to an undirected bipartite graph. Specifically, given a directed graph \mathcal{G} , its bipartite representation (Bang-Jensen & Gutin, 2008) is expressed as:

$$\mathcal{S}(\hat{\mathbf{A}}) := \begin{bmatrix} \mathbf{0} & \hat{\mathbf{A}} \\ \hat{\mathbf{A}}^\top & \mathbf{0} \end{bmatrix} \in \mathbb{R}^{2n \times 2n}. \quad (6)$$

Here, $\mathcal{S}(\hat{\mathbf{A}})$ is a block matrix consisting of $\hat{\mathbf{A}}$ and $\hat{\mathbf{A}}^\top$. It is evident that $\mathcal{S}(\hat{\mathbf{A}})$ represents the adjacency matrix of an undirected bipartite graph with $2n$ nodes. Figure 2 provides two toy examples of directed graphs and their corresponding undirected bipartite graph representations. Notably, the self-loop in $\hat{\mathbf{A}}$ serves a fundamentally different purpose than in GCN (Kipf & Welling, 2017). In this context, the self-loop ensures the connectivity of the bipartite graph. Without the self-loop, as illustrated in graphs (b) and (e) of Figure 2, the graph structure suffers from significant connectivity issues. Based on this, we present the following lemma.

Lemma 4.1. *When omitting degree-based normalization in Equations (4) and (5), the graph convolution of DiGAE is*

$$\left[\mathbf{S}^{(\ell+1)}, \mathbf{T}^{(\ell+1)} \right]^\top = \sigma \left(\mathcal{S}(\hat{\mathbf{A}}) \left[\mathbf{S}^{(\ell)} \mathbf{W}_S^{(\ell)}, \mathbf{T}^{(\ell)} \mathbf{W}_T^{(\ell)} \right]^\top \right).$$

The proof and its extension with degree-based normalization are provided in Appendix B.3. Lemma 4.1 and extension in its proof reveal that the graph convolution of DiGAE essentially corresponds to the GCN convolution applied to the undirected bipartite graph $\mathcal{S}(\hat{\mathbf{A}})$.

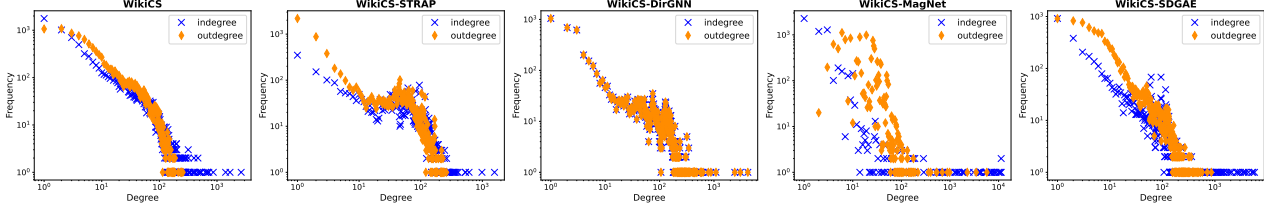


Figure 3. Degree distribution of WikiCS graph and its reconstruction graphs.

4.2. Spectral Directed Graph Auto-Encoder (SDGAE)

Building on our understanding of DiGAE, we identify two main drawbacks. 1) DiGAE struggles to use deep networks for capturing richer structural information due to excessive learnable weight matrices (as highlighted in a recent study on deep GCNs (Peng et al., 2024)). We validate this issue experimentally in the next section. 2) It is difficult to optimize parameters due to heuristic hyperparameters. To address these issues, we propose SDGAE, which uses polynomial weights inspired by spectral-based GNNs (Chien et al., 2021; He et al., 2021) and incorporates symmetric normalization of the adjacency matrix. The convolutional layer of SDGAE is defined as: $[S^{(\ell+1)}, T^{(\ell+1)}]^\top =$

$$\begin{bmatrix} w_S^{(\ell)} \\ w_T^{(\ell)} \end{bmatrix} \odot \begin{bmatrix} \mathbf{0} & \tilde{\mathbf{A}} \\ \tilde{\mathbf{A}}^\top & \mathbf{0} \end{bmatrix} \begin{bmatrix} S^{(\ell)} \\ T^{(\ell)} \end{bmatrix} + \begin{bmatrix} S^{(\ell)} \\ T^{(\ell)} \end{bmatrix}, \quad (7)$$

where $w_S^{(\ell)}, w_T^{(\ell)} \in \mathbb{R}$ are learnable scalar weights, initialized to one. $\tilde{\mathbf{A}} = \hat{\mathbf{D}}_{\text{out}}^{-1/2} \hat{\mathbf{A}} \hat{\mathbf{D}}_{\text{in}}^{-1/2}$ denotes the normalized adjacency matrix, and lemma 4.2 demonstrates that this normalization corresponds to the symmetric normalization of $\mathcal{S}(\hat{\mathbf{A}})$. Each layer of this graph convolution performs weighted propagation over the normalized undirected bipartite graph $\mathcal{S}(\tilde{\mathbf{A}})$, with the addition of a residual connection.

Lemma 4.2. *The symmetrically normalized block adjacency matrix $\mathbf{D}_S^{-1/2} \mathcal{S}(\hat{\mathbf{A}}) \mathbf{D}_S^{-1/2} = \mathcal{S}(\tilde{\mathbf{A}})$, where $\mathbf{D}_S = \text{diag}(\hat{\mathbf{D}}_{\text{out}}, \hat{\mathbf{D}}_{\text{in}})$ is the diagonal degree matrix of $\mathcal{S}(\hat{\mathbf{A}})$.*

The proof of Lemma 4.2 is provided in Appendix B.4. For the initialization of $S^{(0)}$ and $T^{(0)}$ in the implementation, we follow spectral-based GNNs (Chien et al., 2021) and use two MLPs: $S^{(0)} = \text{MLP}_S(\mathbf{X})$ and $T^{(0)} = \text{MLP}_T(\mathbf{X})$. For the decoder, we apply the inner product $\sigma(s_u | t_v)$, as well as MLP scoring functions $\text{MLP}(s_u \odot t_v)$ and $\text{MLP}(s_u | t_v)$.

Table 4 presents SDGAE’s results on DirLinkBench for the Hits@100 metric, where it achieves state-of-the-art performance on four of the seven datasets, while delivering competitive results on the remaining three. Furthermore, SDGAE significantly outperforms DiGAE. These results demonstrate the effectiveness of SDGAE for the directed link prediction task. Additional details and experimental settings for SDGAE are provided in Appendix F.

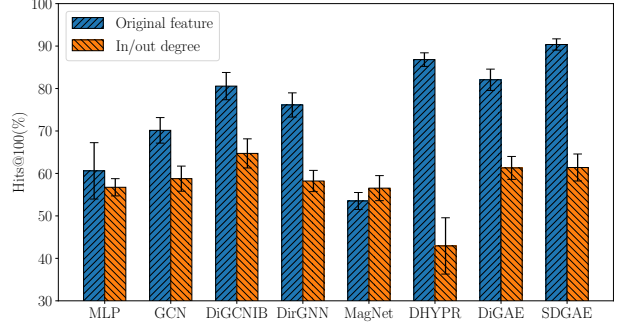


Figure 4. Comparison of various methods’ performance using either the original features or in/out degrees as inputs on Cora-ML.

5. Analysis

In this section, we empirically analyze the factors influencing directed link prediction performance and examine the properties of SDGAE.

5.1. Feature Inputs

We investigate the impact of different feature inputs on GNNs for directed link prediction. Figure 4 presents results on Cora-ML using either original features or in/out degrees as inputs, with additional results for other datasets provided in Appendix G.3.1. Overall, original features enhance performance on most datasets; however, for datasets like WikiCS, in/out degrees prove more effective. Notably, in datasets lacking original features (e.g., Slashdot, Epinions), in/out degrees outperform random features. These findings emphasize the importance of proper feature inputs for improving GNN performance. Enhancing feature quality is a key research direction, especially for datasets with weak or missing original features.

5.2. Loss Function and Decoder

We analyze the impact of different decoders and loss functions on directed link prediction methods. For embedding methods, we compare decoders such as logistic regression (Hamedani et al., 2023) and inner product (Yin & Wei, 2019). For single real-valued GNNs, we evaluate the effects of Cross-Entropy (CE) loss and Binary Cross-Entropy (BCE) loss using decoders like MLP scoring functions (Zhang et al., 2021) and inner product. The corresponding results are provided in Appendix G.3.2.

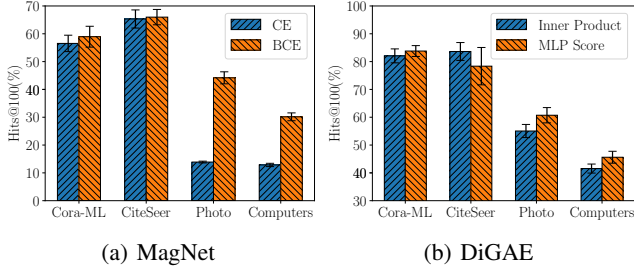


Figure 5. The impact of loss functions and decoders.

In Figure 5(a), we compare the impact of using CE and BCE loss separately on MagNet’s performance, showing that BCE loss consistently outperforms CE loss. This trend aligns with findings from other methods in Appendix G.3.2. These results suggest shortcomings in previous approaches that relied on CE loss (He et al., 2023), as link prediction is fundamentally a binary classification task where BCE loss provides clear advantages (Li et al., 2023). In Figure 5(b), we compare two decoders—inner product and MLP score for DiGAE, and find that MLP score performs better on three datasets. These results above highlight two insights: 1) decoder design significantly impacts model performance, as emphasized in Corollary 2.3, and 2) BCE loss is more effective for link prediction tasks. Furthermore, the poor performance of MagNet and DUPLEX may be attributed to their reliance on CE loss and unsuitable decoders.

5.3. Degree Distribution

We assess how well different models preserve the asymmetry of directed graphs by analyzing their degree distributions. Following STRAP (Yin & Wei, 2019), we compute every edge probability for each model and select the top- m' edges—where m' is the number of edges in the training graph—to reconstruct it. Figure 3 compares the true in-/out-degree distributions of the WikiCS training graph with those of reconstructed graphs generated by four various methods. Results show that STRAP and SDGAE best preserve the degree distributions, with STRAP excelling at in-degrees, explaining its superior performance on WikiCS. DirGNN, using the decoder $\text{MLP}(\mathbf{h}_u \odot \mathbf{h}_v)$, produces identical in-/out-degree distributions but still captures in-degrees correctly. In contrast, MagNet fails to learn valid distributions, leading to poor performance. Additionally, incorporating in-/out-degrees as feature inputs enhances degree distributions, as shown in Appendix G.3.3. These findings underscore the need for GNNs to better preserve degree distributions, an underexplored challenge compared to embedding methods.

5.4. SDGAE versus DiGAE

We investigate which aspects of SDGAE contribute to its performance gains over DiGAE. Figure 6 shows that SDGAE benefits from deep graph convolutions, achiev-

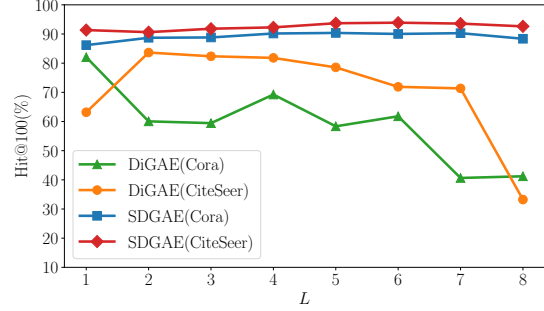


Figure 6. Performance comparison of SDGAE and DiGAE on Cora-ML and CiteSeer with increasing convolutional layers.

ing optimal performance at $L = 5$, whereas DiGAE’s performance declines with increasing layers due to excessive learnable weight matrices (Peng et al., 2024). Figure 5(b) further demonstrates that improving DiGAE’s decoder enhances performance, underscoring the importance of decoder design. Additionally, adjacency matrix normalization, $\hat{\mathbf{D}}_{\text{out}}^{-1/2} \hat{\mathbf{A}} \hat{\mathbf{D}}_{\text{in}}^{-1/2}$, is not a decisive factor, as shown in Appendix G.3.4. Overall, our SDGAE’s advantage over DiGAE stems primarily from the effective deep graph convolutions and well-designed decoder.

5.5. Metric and Negative Sampling Strategy

In Appendix G.3.5, we compare baseline results across different metrics, showing that Accuracy, AUC, and AP exhibit small performance gaps between methods. Notably, many simple undirected graph GNNs achieving high accuracy. These findings suggest that ranking metrics better capture model performance for link prediction, as observed in undirected graphs (Yang et al., 2015). Additionally, we analyze the impact of negative edge sampling strategies during training and find that they significantly influence model performance. Exploring more sampling strategies, inspired by advancements in undirected graph link prediction (Li et al., 2023), could be a promising direction for future research.

6. Conclusion

This paper presents a unified framework for directed link prediction, highlighting the critical role of dual embeddings and decoder design. To address existing limitations, we introduce DirLinkBench, a robust benchmark for evaluating directed link prediction methods. Results on the new benchmark reveal that current methods exhibit inconsistent performance, while our proposed SDGAE achieves state-of-the-art performance. Based on our findings, we highlight two key open challenges: 1) *How can more efficient decoders be developed for complex-valued methods?* 2) *How can GNNs better preserve in-/out-degree distributions?* We hope this work inspires further advancements in directed link prediction and contributes to the development of more effective and theoretically grounded models.

References

- Bang-Jensen, J. and Gutin, G. Z. *Digraphs: theory, algorithms and applications*. Springer Science & Business Media, 2008.
- Bhuyan, M. H., Bhattacharyya, D. K., and Kalita, J. K. Network anomaly detection: methods, systems and tools. *Ieee communications surveys & tutorials*, 16(1):303–336, 2013.
- Bojchevski, A. and Günnemann, S. Deep gaussian embedding of graphs: Unsupervised inductive learning via ranking. In *ICLR*, 2018.
- Chien, E., Peng, J., Li, P., and Milenkovic, O. Adaptive universal generalized pagerank graph neural network. In *ICLR*, 2021.
- Fey, M. and Lenssen, J. E. Fast graph representation learning with pytorch geometric. *arXiv preprint arXiv:1903.02428*, 2019.
- Fiorini, S., Coniglio, S., Ciavotta, M., and Messina, E. Sigmanet: One laplacian to rule them all. In *AAAI*, pp. 7568–7576, 2023.
- Gasteiger, J., Bojchevski, A., and Günnemann, S. Predict then propagate: Graph neural networks meet personalized pagerank. In *ICLR*, 2019.
- Geisler, S., Li, Y., Mankowitz, D. J., Cemgil, A. T., Günnemann, S., and Paduraru, C. Transformers meet directed graphs. In *ICML*, pp. 11144–11172. PMLR, 2023.
- Golub, G. H. and Van Loan, C. F. *Matrix computations*. JHU press, 2013.
- Hamedani, M. R., Ryu, J.-S., and Kim, S.-W. Eltra: An embedding method based on learning-to-rank to preserve asymmetric information in directed graphs. In *CIKM*, pp. 2116–2125, 2023.
- He, M., Wei, Z., Xu, H., et al. Bernnet: Learning arbitrary graph spectral filters via bernstein approximation. *NeurIPS*, 34:14239–14251, 2021.
- He, M., Wei, Z., and Wen, J.-R. Convolutional neural networks on graphs with chebyshev approximation, revisited. *NeurIPS*, 35:7264–7276, 2022.
- He, Y., Zhang, X., Huang, J., Rozemberczki, B., Cucuringu, M., and Reinert, G. Pytorch geometric signed directed: A software package on graph neural networks for signed and directed graphs. In *LoG*, 2023.
- Hu, W., Fey, M., Zitnik, M., Dong, Y., Ren, H., Liu, B., Catasta, M., and Leskovec, J. Open graph benchmark: Datasets for machine learning on graphs. *NeurIPS*, 33: 22118–22133, 2020.
- Huang, J., Mo, Y., Hu, P., Shi, X., Yuan, S., Zhang, Z., and Zhu, X. Exploring the role of node diversity in directed graph representation learning. In *IJCAI*, pp. 2072–2080, 2024.
- Katz, L. A new status index derived from sociometric analysis. *Psychometrika*, 18(1):39–43, 1953.
- Ke, Z., Yu, H., Li, J., and Zhang, H. DUPLEX: Dual GAT for complex embedding of directed graphs. In *ICML*, pp. 23430–23448, 2024.
- Khosla, M., Leonhardt, J., Nejd, W., and Anand, A. Node representation learning for directed graphs. In *ECML PKDD*, pp. 395–411. Springer, 2020.
- Kipf, T. N. and Welling, M. Semi-supervised classification with graph convolutional networks. In *ICLR*, 2017.
- Koke, C. and Cremers, D. Holonets: Spectral convolutions do extend to directed graphs. In *ICLR*, 2024.
- Kollias, G., Kalantzis, V., Idé, T., Lozano, A., and Abe, N. Directed graph auto-encoders. In *AAAI*, pp. 7211–7219, 2022.
- Leskovec, J. and Sosič, R. Snap: A general-purpose network analysis and graph-mining library. *ACM Transactions on Intelligent Systems and Technology (TIST)*, 8(1):1–20, 2016.
- Li, J., Shomer, H., Mao, H., Zeng, S., Ma, Y., Shah, N., Tang, J., and Yin, D. Evaluating graph neural networks for link prediction: Current pitfalls and new benchmarking. In *NeurIPS*, 2023.
- Li, X., Liao, M., Wu, Z., Su, D., Zhang, W., Li, R.-H., and Wang, G. Lightdic: A simple yet effective approach for large-scale digraph representation learning. *Proceedings of the VLDB Endowment*, 17(7):1542–1551, 2024.
- Liben-Nowell, D. and Kleinberg, J. The link prediction problem for social networks. In *CIKM*, pp. 556–559, 2003.
- Lin, L. and Gao, J. A magnetic framelet-based convolutional neural network for directed graphs. In *ICASSP*, pp. 1–5. IEEE, 2023.
- Liu, L., Chen, K.-J., and Liu, Z. Collaborative bi-aggregation for directed graph embedding. *Neural Networks*, 164:707–718, 2023.

- Maskey, S., Paolino, R., Bacho, A., and Kutyniok, G. A fractional graph laplacian approach to oversmoothing. In *NeurIPS*, 2023.
- Massa, P. and Avesani, P. Controversial users demand local trust metrics: An experimental study on epinions. com community. In *AAAI*, volume 1, pp. 121–126, 2005.
- McCallum, A. K., Nigam, K., Rennie, J., and Seymore, K. Automating the construction of internet portals with machine learning. *Information Retrieval*, 3:127–163, 2000.
- Mernyei, P. and Cangea, C. Wiki-cs: A wikipedia-based benchmark for graph neural networks. *arXiv preprint arXiv:2007.02901*, 2020.
- Monti, F., Otness, K., and Bronstein, M. M. Motifnet: a motif-based graph convolutional network for directed graphs. In *2018 IEEE Data Science Workshop (DSW)*, pp. 225–228. IEEE, 2018.
- Ordozgoiti, B., Matakos, A., and Gionis, A. Finding large balanced subgraphs in signed networks. In *Proceedings of The Web Conference 2020*, pp. 1378–1388, 2020.
- Ou, M., Cui, P., Pei, J., Zhang, Z., and Zhu, W. Asymmetric transitivity preserving graph embedding. In *KDD*, pp. 1105–1114, 2016.
- Page, L., Brin, S., Motwani, R., and Winograd, T. The pagerank citation ranking : Bringing order to the web. In *The Web Conference*, 1999.
- Peng, J., Lei, R., and Wei, Z. Beyond over-smoothing: Uncovering the trainability challenges in deep graph neural networks. In *CIKM*, pp. 1878–1887, 2024.
- Rendle, S., Freudenthaler, C., Gantner, Z., and Schmidt-Thieme, L. Bpr: Bayesian personalized ranking from implicit feedback. In *UAI*, pp. 452–461, 2009.
- Rossi, E., Charpentier, B., Di Giovanni, F., Frasca, F., Günnemann, S., and Bronstein, M. M. Edge directionality improves learning on heterophilic graphs. In *Learning on Graphs Conference*, pp. 25–1. PMLR, 2024.
- Salha, G., Limnios, S., Hennequin, R., Tran, V.-A., and Vazirgiannis, M. Gravity-inspired graph autoencoders for directed link prediction. In *CIKM*, pp. 589–598, 2019.
- Sen, P., Namata, G., Bilgic, M., Getoor, L., Galligher, B., and Eliassi-Rad, T. Collective classification in network data. *AI magazine*, 29(3):93–93, 2008.
- Shchur, O., Mumme, M., Bojchevski, A., and Günnemann, S. Pitfalls of graph neural network evaluation. *Relational Representation Learning Workshop, NeurIPS 2018*, 2018.
- Tong, Z., Liang, Y., Sun, C., Li, X., Rosenblum, D., and Lim, A. Digraph inception convolutional networks. *NeurIPS*, 33:17907–17918, 2020a.
- Tong, Z., Liang, Y., Sun, C., Rosenblum, D. S., and Lim, A. Directed graph convolutional network. *arXiv preprint arXiv:2004.13970*, 2020b.
- Veličković, P., Cucurull, G., Casanova, A., Romero, A., Liò, P., and Bengio, Y. Graph attention networks. In *ICLR*, 2018.
- Virinchi, S. and Saladi, A. Blade: Biased neighborhood sampling based graph neural network for directed graphs. In *WSDM*, pp. 42–50, 2023.
- Weisfeiler, B. and Leman, A. The reduction of a graph to canonical form and the algebra which appears therein. *nti, Series*, 2(9):12–16, 1968.
- Yang, Y., Lichtenwalter, R. N., and Chawla, N. V. Evaluating link prediction methods. *Knowledge and Information Systems*, 45:751–782, 2015.
- Yin, Y. and Wei, Z. Scalable graph embeddings via sparse transpose proximities. In *KDD*, pp. 1429–1437, 2019.
- Yoo, H., Lee, Y.-C., Shin, K., and Kim, S.-W. Disentangling degree-related biases and interest for out-of-distribution generalized directed network embedding. In *Proceedings of the ACM Web Conference 2023*, pp. 231–239, 2023.
- Zhang, M. and Chen, Y. Link prediction based on graph neural networks. *NeurIPS*, 31, 2018.
- Zhang, X., He, Y., Brugnone, N., Perlmutter, M., and Hirn, M. Magnet: A neural network for directed graphs. *NeurIPS*, 34:27003–27015, 2021.
- Zhang, Z., Cui, P., Wang, X., Pei, J., Yao, X., and Zhu, W. Arbitrary-order proximity preserved network embedding. In *KDD*, pp. 2778–2786, 2018.
- Zhou, C., Liu, Y., Liu, X., Liu, Z., and Gao, J. Scalable graph embedding for asymmetric proximity. In *AAAI*, 2017.
- Zhou, H., Chegu, A., Sohn, S. S., Fu, Z., De Melo, G., and Kapadia, M. D-hypr: Harnessing neighborhood modeling and asymmetry preservation for digraph representation learning. In *CIKM*, pp. 2732–2742, 2022.
- Zhu, S., Li, J., Peng, H., Wang, S., and He, L. Adversarial directed graph embedding. In *AAAI*, pp. 4741–4748, 2021.

Appendix Contents

- Appendix A: Notation p.12
- Appendix B: Proof p.12
 - B.1: The proof of Theorem 2.2 p.12
 - B.2: The proof of Corollary 2.3 p.13
 - B.3: The proof of Lemma 4.1 p.13
 - B.4: The proof of Lemma 4.2 p.14
- Appendix C: Related Work p.14
- Appendix D: Details of Unified Framework p.15
- Appendix E: Issues with Existing Experimental Setup p.16
 - E.1: Details of multiple subtask setup p.16
 - E.2: Details of experimental setting and more results p.16
- Appendix F: Details and Experimental Setting for SDGAE p.17
 - F.1: More details of graph convolution p.17
 - F.2: Experimental setting p.18
- Appendix G: More Details of DirLinkBench p.18
 - G.1: Datasets and baselines p.18
 - G.2: Metric description p.20
 - G.3: Additional results in analysis p.20
- Appendix H: Complete Results of DirLinkBench on Seven Datasets p.24
 - H.1: Results on Cora-ML p.24
 - H.2: Results on CiteSeer p.25
 - H.3: Results on Photo p.26
 - H.4: Results on Computers p.27
 - H.5: Results on WikiCS p.28
 - H.6: Results on Slashdot p.29
 - H.7: Results on Epinions p.30

A. Notation

We summarize the main notations of the paper in Table 5.

Table 5. Summation of main notations in this paper.

Notation	Description
$\mathcal{G} = (V, E)$	directed unweighted graph with node set V and edge set E .
n, m	the number of nodes and edges, $n = V $ and $m = E $.
\mathbf{A}	the adjacency matrix of \mathcal{G} , $\mathbf{A}_{uv} = 1$ for a edge from node u to v , and $\mathbf{A}_{uv} = 0$ otherwise.
\mathbf{H}	the Hermitian adjacency matrix, defined as $\mathbf{H} = \mathbf{A}_s \odot \exp(i\frac{\pi}{2}\mathbf{\Theta})$.
\mathbf{A}_s	the adjacency matrix of the undirected graph derived from \mathcal{G} , $\mathbf{A}_s = \mathbf{A} \cup \mathbf{A}^\top$.
$\mathbf{\Theta}$	the skew-symmetric matrix $\mathbf{\Theta} = \mathbf{A} - \mathbf{A}^\top$.
$\mathbf{D}_{\text{out}}, \mathbf{D}_{\text{int}}$	the out- and in-degree matrix of \mathbf{A} , $\mathbf{D}_{\text{out}} = \text{diag}(\mathbf{A}\mathbf{1})$ and $\mathbf{D}_{\text{int}} = \text{diag}(\mathbf{A}^\top\mathbf{1})$.
\mathbf{X}	the node feature matrix, $\mathbf{X} \in \mathbb{R}^{n \times d'}$ and d' is the dimension.
θ_u, ϕ_u	real-valued dual embeddings $\theta_u \in \mathbb{R}^{d_\theta}$, $\phi_u \in \mathbb{R}^{d_\phi}$, d_θ, d_ϕ are the dimensions.
$p(u, v)$	the probability of directed edge (u, v) existing.
$\mathcal{G}' = (V, E')$	the observed/training graph with node set V and edge set E' .
$\hat{\mathbf{A}}$	the adjacency matrix with added self-loops, $\hat{\mathbf{A}} = \mathbf{A} + \mathbf{I}$.
$\hat{\mathbf{D}}_{\text{out}}, \hat{\mathbf{D}}_{\text{int}}$	the out- and in-degree matrix of $\hat{\mathbf{A}}$.
$\mathcal{S}(\hat{\mathbf{A}})$	the block matrix consisting of $\hat{\mathbf{A}}$ and $\hat{\mathbf{A}}^\top$.
$\tilde{\mathbf{A}}$	the normalized adjacency matrix, $\tilde{\mathbf{A}} = \hat{\mathbf{D}}_{\text{out}}^{-1/2} \hat{\mathbf{A}} \hat{\mathbf{D}}_{\text{int}}^{-1/2}$.
\odot, \parallel	the Hadamard product and concatenation process.
d, d'	the dimension of embeddings and feature matrix.

B. Proof

B.1. The proof of Theorem 2.2

Theorem 2.2. For the framework defined by Equations (2) and (3), if $d_\theta, d_\phi > 0$ and sufficiently large, there exist embeddings θ_u, ϕ_u and a decoder $\text{Dec}(\cdot)$ that can correctly compute the probability $p(u, v)$ of any directed edge (u, v) in an arbitrary graph. Conversely, if $d_\theta = 0$ or $d_\phi = 0$, no such embeddings or decoders can compute the correct probability of any edges in an arbitrary graph.

Proof. If $d_\theta, d_\phi > 0$ and are sufficiently large, there exist two real-valued embeddings, θ_u and ϕ_u , for each node u in the graph. According to the unified framework for directed link prediction methods, these embeddings, θ_u and ϕ_u , can represent the outputs of various encoder methods, including source-target methods, complex-valued methods, and gravity-inspired methods. For these encoder methods, a decoder exists that can compute the probability $p(u, v)$ for any directed edge (u, v) . As an example, consider source-target methods. If we have two embeddings, s_u and t_u , for each node u , we can correctly compute the probability $p(u, v)$ of any edge (u, v) using the expression $p(u, v) = \sigma(s_u^\top t_v)$, when $\mathbf{A}_{uv} = s_u^\top t_v$. Based on existing embedding methods such as STRAP and HOPE (Yin & Wei, 2019; Ou et al., 2016), it is known that there exist embeddings s_u and t_v that satisfy $\mathbf{A}_{uv} = s_u^\top t_v$. For complex-valued methods, such as DUPLEX (Ke et al., 2024), it has been demonstrated that there exist embeddings z_u and z_v such that $\mathbf{H}_{uv} = z_u \bar{z}_v$, where \bar{z}_v is the complex conjugate of z_v . Therefore, we conclude that there exist embeddings θ_u and ϕ_u , along with a decoder $\text{Dec}(\cdot)$, that can correctly compute the probability $p(u, v)$ for any directed edge (u, v) in an arbitrary graph.

If $d_\theta = 0$ or $d_\phi = 0$, this implies that each node u in the graph is represented by a single real-valued embedding h_u .

According to existing methods (Zhang et al., 2021; He et al., 2023), there are three main types of decoders for single real-valued embeddings: $\sigma(\mathbf{h}_u^\top \mathbf{h}_v)$, $\text{MLP}(\mathbf{h}_u \odot \mathbf{h}_v)$, and $\text{MLP}(\mathbf{h}_u \parallel \mathbf{h}_v)$. For the decoders $\sigma(\mathbf{h}_u^\top \mathbf{h}_v)$ and $\text{MLP}(\mathbf{h}_u \odot \mathbf{h}_v)$, it is known that they cannot distinguish between $p(u, v)$ and $p(v, u)$. This is because $\mathbf{h}_v^\top \mathbf{h}_u = \mathbf{h}_u^\top \mathbf{h}_v$ and $\mathbf{h}_u \odot \mathbf{h}_v = \mathbf{h}_v \odot \mathbf{h}_u$, which leads to $p(u, v) = p(v, u)$. As a result, these decoders fail to compute the correct probabilities for directed edges.

Next, we demonstrate that the decoder $\text{MLP}(\mathbf{h}_u \parallel \mathbf{h}_v)$ also fails to compute the probability $p(u, v)$ for certain graphs. Consider the directed ring graph (a) in Figure 2, which consists of three nodes and three edges ($1 \rightarrow 2, 2 \rightarrow 3, 3 \rightarrow 1$). Each node is assigned a real-valued embedding, i.e., $\mathbf{h}_1, \mathbf{h}_2, \mathbf{h}_3$. Let the decoder be a simple MLP with $\sigma = \text{Sigmoid}(\cdot)$ as the activation function. For edge $1 \rightarrow 2$, the probability is given by:

$$p(1, 2) = \sigma(\mathbf{h}_1 \mathbf{w}_1 + \mathbf{h}_2 \mathbf{w}_2) > 0.5, \quad p(2, 1) = \sigma(\mathbf{h}_2 \mathbf{w}_1 + \mathbf{h}_1 \mathbf{w}_2) < 0.5. \quad (8)$$

Here, $\mathbf{w}_1, \mathbf{w}_2 \in \mathbb{R}^{d \times 1}$ are the learnable weights, and d is the dimensionality of \mathbf{h} . From these inequalities, we have:

$$\mathbf{h}_1 \mathbf{w}_1 + \mathbf{h}_2 \mathbf{w}_2 > 0, \quad \mathbf{h}_2 \mathbf{w}_1 + \mathbf{h}_1 \mathbf{w}_2 < 0. \quad (9)$$

Subtracting the second inequality from the first gives:

$$(\mathbf{h}_1 - \mathbf{h}_2) \mathbf{w}_1 + (\mathbf{h}_2 - \mathbf{h}_1) \mathbf{w}_2 > 0. \quad (10)$$

Similarly, for edges $2 \rightarrow 3$ and $3 \rightarrow 1$, we derive:

$$(\mathbf{h}_2 - \mathbf{h}_3) \mathbf{w}_1 + (\mathbf{h}_3 - \mathbf{h}_2) \mathbf{w}_2 > 0, \quad (\mathbf{h}_3 - \mathbf{h}_1) \mathbf{w}_1 + (\mathbf{h}_1 - \mathbf{h}_3) \mathbf{w}_2 > 0. \quad (11)$$

Adding these three inequalities, including Eq. (10), results in $0 > 0$, which is a contradiction. Therefore, no embeddings \mathbf{h} and weights \mathbf{w} exist that can satisfy this condition. The same result holds even if nonlinearities are added to the MLP. This example demonstrates that the decoder $\text{MLP}(\mathbf{h}_u \parallel \mathbf{h}_v)$ also fails to compute the probabilities for directed edges in an arbitrary graph. Hence, for existing methods, if $d_\theta = 0$ or $d_\phi = 0$, no embeddings or decoders can correctly compute the probabilities for any edges in an arbitrary graph. \square

B.2. The proof of Corollary 2.3

Corollary 2.3. With dual embeddings θ_u and ϕ_u , if there is no suitable decoder $\text{Dec}(\cdot)$, the probability $p(u, v)$ of any edge (u, v) cannot be computed correctly. In contrast, even with one single embedding (θ_u or $\phi_u = \emptyset$), a suitable decoder can improve the ability to compute edge probabilities.

Proof. Theorem 2.2 establishes that dual embeddings (θ_u, ϕ_u) combined with a suitable decoder $\text{Dec}(\cdot)$, guarantee the correct computation of $p(u, v)$. However, if the decoder is unsuitable (e.g., it fails to model directional relationships), even valid embeddings cannot produce correct edge probabilities. For example, a symmetric decoder like $\text{Dec}(\theta_u, \phi_u, \theta_v, \phi_v) = \sigma(\theta_u^\top \theta_v + \phi_u^\top \phi_v)$ leads to $p(u, v) = p(v, u)$, which violates directionality. This highlights that the decoder must align with the embeddings' structure to exploit their expressivity fully.

In contrast, Theorem 2.2 shows that single embeddings ($d_\theta = 0$ or $d_\phi = 0$) cannot universally represent arbitrary directed graphs. Nevertheless, a suitable decoder can still improve edge probability estimation in constrained scenarios. For example, an asymmetric decoder like $\text{Dec}(\mathbf{h}_u, \mathbf{h}_v) = \text{MLP}(\mathbf{h}_u \parallel \mathbf{h}_v)$ can preserve some directionality by learning from the data. While such decoders fail on more complex structures like ring graphs (as shown in Theorem 2.2), they can handle simpler directed graph structures. In summary, dual embeddings require suitable decoders to achieve theoretical expressivity, while single embeddings, though fundamentally limited, can still benefit from specific decoders in practice. \square

B.3. The proof of Lemma 4.1

Lemma 4.1. When omitting degree-based normalization in Equations (4) and (5), the graph convolution of DiGAE is

$$\left[\mathbf{S}^{(\ell+1)}, \mathbf{T}^{(\ell+1)} \right]^\top = \sigma \left(\mathcal{S}(\hat{\mathbf{A}}) \left[\mathbf{S}^{(\ell)} \mathbf{W}_S^{(\ell)}, \mathbf{T}^{(\ell)} \mathbf{W}_T^{(\ell)} \right]^\top \right).$$

Proof. Substituting the block matrix $\mathcal{S}(\hat{\mathbf{A}}) = \begin{bmatrix} \mathbf{0} & \hat{\mathbf{A}} \\ \hat{\mathbf{A}}^\top & \mathbf{0} \end{bmatrix}$ into the above convolution equation, we obtain:

$$\begin{bmatrix} \mathbf{S}^{(\ell+1)} \\ \mathbf{T}^{(\ell+1)} \end{bmatrix} = \sigma \left(\begin{bmatrix} \mathbf{0} & \hat{\mathbf{A}} \\ \hat{\mathbf{A}}^\top & \mathbf{0} \end{bmatrix} \begin{bmatrix} \mathbf{S}^{(\ell)} \mathbf{W}_S^{(\ell)} \\ \mathbf{T}^{(\ell)} \mathbf{W}_T^{(\ell)} \end{bmatrix} \right) = \begin{bmatrix} \sigma \left(\hat{\mathbf{A}} \mathbf{T}^{(\ell)} \mathbf{W}_T^{(\ell)} \right) \\ \sigma \left(\hat{\mathbf{A}}^\top \mathbf{S}^{(\ell)} \mathbf{W}_S^{(\ell)} \right) \end{bmatrix}. \quad (12)$$

This result corresponds exactly to Equations (4) and (5) when the degree-based normalization of $\hat{\mathbf{A}}$ is not considered. If we include the normalization, it actually applies to $\mathcal{S}(\hat{\mathbf{A}})$. Notably, the diagonal degree matrix of $\mathcal{S}(\hat{\mathbf{A}})$ is given by $\text{diag}(\hat{\mathbf{D}}_{\text{out}}, \hat{\mathbf{D}}_{\text{in}})$. Therefore, we have:

$$\begin{bmatrix} \mathbf{S}^{(\ell+1)} \\ \mathbf{T}^{(\ell+1)} \end{bmatrix} = \sigma \left(\begin{bmatrix} \hat{\mathbf{D}}_{\text{out}}^{-\beta} & \mathbf{0} \\ \mathbf{0} & \hat{\mathbf{D}}_{\text{in}}^{-\alpha} \end{bmatrix} \begin{bmatrix} \mathbf{0} & \hat{\mathbf{A}} \\ \hat{\mathbf{A}}^\top & \mathbf{0} \end{bmatrix} \begin{bmatrix} \hat{\mathbf{D}}_{\text{out}}^{-\beta} & \mathbf{0} \\ \mathbf{0} & \hat{\mathbf{D}}_{\text{in}}^{-\alpha} \end{bmatrix} \begin{bmatrix} \mathbf{S}^{(\ell)} \mathbf{W}_S^{(\ell)} \\ \mathbf{T}^{(\ell)} \mathbf{W}_T^{(\ell)} \end{bmatrix} \right) \quad (13)$$

$$= \begin{bmatrix} \sigma \left(\hat{\mathbf{D}}_{\text{out}}^{-\beta} \hat{\mathbf{A}} \hat{\mathbf{D}}_{\text{in}}^{-\alpha} \mathbf{T}^{(\ell)} \mathbf{W}_T^{(\ell)} \right) \\ \sigma \left(\hat{\mathbf{D}}_{\text{in}}^{-\alpha} \hat{\mathbf{A}}^\top \hat{\mathbf{D}}_{\text{out}}^{-\beta} \mathbf{S}^{(\ell)} \mathbf{W}_S^{(\ell)} \right) \end{bmatrix}. \quad (14)$$

This result aligns exactly with the graph convolution of DiGAE in Equations (4) and (5). \square

B.4. The proof of Lemma 4.2

Lemma 4.2. The symmetrically normalized block adjacency matrix $D_S^{-1/2} \mathcal{S}(\hat{\mathbf{A}}) D_S^{-1/2} = \mathcal{S}(\tilde{\mathbf{A}})$, where $D_S = \text{diag}(\hat{\mathbf{D}}_{\text{out}}, \hat{\mathbf{D}}_{\text{in}})$ is the diagonal degree matrix of $\mathcal{S}(\hat{\mathbf{A}})$.

Proof. For the block adjacency matrix $\mathcal{S}(\hat{\mathbf{A}}) = \begin{bmatrix} \mathbf{0} & \hat{\mathbf{A}} \\ \hat{\mathbf{A}}^\top & \mathbf{0} \end{bmatrix}$ and its degree matrix $D_S = \begin{bmatrix} \hat{\mathbf{D}}_{\text{out}} & \mathbf{0} \\ \mathbf{0} & \hat{\mathbf{D}}_{\text{in}} \end{bmatrix}$, we have

$$D_S^{-1/2} \mathcal{S}(\hat{\mathbf{A}}) D_S^{-1/2} = \begin{bmatrix} \hat{\mathbf{D}}_{\text{out}} & \mathbf{0} \\ \mathbf{0} & \hat{\mathbf{D}}_{\text{in}} \end{bmatrix}^{-1/2} \begin{bmatrix} \mathbf{0} & \hat{\mathbf{A}} \\ \hat{\mathbf{A}}^\top & \mathbf{0} \end{bmatrix} \begin{bmatrix} \hat{\mathbf{D}}_{\text{out}} & \mathbf{0} \\ \mathbf{0} & \hat{\mathbf{D}}_{\text{in}} \end{bmatrix}^{-1/2} \quad (15)$$

$$= \begin{bmatrix} \hat{\mathbf{D}}_{\text{out}}^{-1/2} & \mathbf{0} \\ \mathbf{0} & \hat{\mathbf{D}}_{\text{in}}^{-1/2} \end{bmatrix} \begin{bmatrix} \mathbf{0} & \hat{\mathbf{A}} \\ \hat{\mathbf{A}}^\top & \mathbf{0} \end{bmatrix} \begin{bmatrix} \hat{\mathbf{D}}_{\text{out}}^{-1/2} & \mathbf{0} \\ \mathbf{0} & \hat{\mathbf{D}}_{\text{in}}^{-1/2} \end{bmatrix} \quad (16)$$

$$= \begin{bmatrix} \mathbf{0} & \hat{\mathbf{D}}_{\text{out}}^{-1/2} \hat{\mathbf{A}} \hat{\mathbf{D}}_{\text{in}}^{-1/2} \\ \left(\hat{\mathbf{D}}_{\text{out}}^{-1/2} \hat{\mathbf{A}} \hat{\mathbf{D}}_{\text{in}}^{-1/2} \right)^\top & \mathbf{0} \end{bmatrix} \quad (17)$$

$$= \begin{bmatrix} \mathbf{0} & \tilde{\mathbf{A}} \\ \tilde{\mathbf{A}}^\top & \mathbf{0} \end{bmatrix} \quad (18)$$

$$= \mathcal{S}(\tilde{\mathbf{A}}). \quad (19)$$

\square

C. Related Work

Existing methods for directed link prediction can be broadly categorized into embedding methods and graph neural networks (GNNs). We review these methods below and discuss their relevance to our work.

Embedding Methods for directed graphs primarily aim to capture asymmetric relationships. Most approaches generate two vectors per node: a source embedding (s_u) and a target embedding (t_u). These embeddings are learned using either factorization or random walks. Factorization-based methods include HOPE (Ou et al., 2016), which applies the Katz similarity (Katz, 1953) followed by singular value decomposition (SVD) (Golub & Van Loan, 2013), and AROPE (Zhang et al., 2018), which generalizes this idea to preserve arbitrary-order proximities. STRAP (Yin & Wei, 2019) combines Personalized PageRank (PPR) (Page et al., 1999) scores from both the original and transposed graphs before applying SVD. Random-walk methods include APP (Zhou et al., 2017), which trains embeddings using PPR-based random walks,

and NERD (Khosla et al., 2020), which samples nodes according to degree distributions. Additional techniques include DGGAN (Zhu et al., 2021) (adversarial training), ELTRA (Hamedani et al., 2023) (ranking-based learning), and ODIN (Yoo et al., 2023) (degree bias separation). These methods all focus on generating source–target embeddings from graph structures for link prediction tasks.

Graph Neural Networks for directed graphs can be classified into four main categories based on their embedding strategies: 1) Source–target methods learn separate source and target embeddings per node. DiGAE (Kollias et al., 2022) applies GCN (Kipf & Welling, 2017) to both the adjacency and its transpose. CoBA (Liu et al., 2023) aggregates source and target neighbors jointly. BLADE (Virinchi & Saladi, 2023) uses an asymmetric loss to generate dual embeddings from local neighborhoods. 2) Gravity-inspired methods are motivated by Newton’s law of universal gravitation, learning real-valued embeddings alongside a scalar mass parameter. Gravity GAE (Salha et al., 2019) pairs a gravity-based decoder with a GCN-based encoder, while DHYPR (Zhou et al., 2022) extends it via hyperbolic collaborative learning. 3) Single real-valued methods learn a single real-valued embedding for each node. DGCN (Tong et al., 2020b) defines a directed Laplacian using first-/second-order proximities. MotifNet (Monti et al., 2018) leverages motif-based Laplacians. DiGCN and DiGCNIB (Tong et al., 2020a) use Personalized PageRank (PPR) to generalize directed Laplacians. DirGNN (Rossi et al., 2024) develops a flexible convolution for any message-passing neural network (MPNN), and HoloNets (Koke & Cremers, 2024) applies holomorphic functional calculus, employing a network structure similar to DirGNN. 4) Complex-valued methods employ Hermitian adjacency matrices for learning complex embeddings. MagNet (Zhang et al., 2021) defines a magnetic Laplacian to design directed graph convolution. LightDiC (Li et al., 2024) extends MagNet’s convolution to large graphs using a decoupled approach. DUPLEX (Ke et al., 2024) uses dual GAT encoders with Hermitian adjacency. Other directed GNNs include adapting Transformers for directed graphs (Geisler et al., 2023) and extending oversmoothing analyses to directed graphs (Maskey et al., 2023). While these methods define various directed graph convolutions and propagation mechanisms, a fair evaluation in link prediction tasks is often missing. Many methods omit important baselines or suffer from setup limitations (e.g., label leakage). These challenges motivate the work presented in this paper.

D. Details of Unified Framework

Table 6. The unified framework for directed link prediction methods.

Encoder $\text{Enc}(\cdot)$	Embeddings (θ_u, ϕ_u)	Possible Decoder $\text{Dec}(\cdot)$
Source–target	$s_u = \theta_u, \quad t_u = \phi_u$	$\sigma(s_u^\top t_v); \quad \text{LR}(s_u \odot t_v); \quad \text{LR}(s_u \ t_v)$
Single real-valued	$h_u = \theta_u, \quad \emptyset = \phi_u$	$\sigma(h_u^\top h_v); \quad \text{MLP}(h_u \odot h_v); \quad \text{MLP}(h_u \ h_v)$
Complex-valued	$z_u = \theta_u \odot \exp(i\phi_u)$	$\text{Direc}(z_u, z_v); \quad \text{MLP}(\theta_u \ \theta_v \ \phi_u \ \phi_v)$
Gravity-inspired	$h_u = \theta_u, \quad m_u = g(\phi_u)$	$\sigma(m_v - \lambda \log \ h_u - h_v\ _2^2); \quad \sigma(m_v - \lambda \log(\text{dist}_{\mathbb{D}_c^{d'}}(h_u, h_v)))$

Here, we introduce the details of the examples within our unified learning framework for directed link prediction methods. For readability, we copy Table 2 from the main paper in Table 6. Here, σ represents the activation function (e.g., Sigmoid), while LR and MLP denote the logistic regression predictor and the multilayer perceptron, respectively. The symbols \odot and $\|$ represent the Hadamard product and the vector concatenation process, respectively.

For source–target encoder, we define the source embedding as $s_u = \theta_u$ and the target embedding as $t_u = \phi_u$ for each node $u \in V$. Possible decoders include: $\sigma(s_u^\top t_v)$, $\text{LR}(s_u \odot t_v)$, $\text{LR}(s_u \| t_v)$. Here, $s_u^\top t_v$ denotes the inner product of the source and target embeddings, while $\text{LR}(\cdot)$ represents the logistic regression predictor.

For single real-valued encoder, we define the real-valued embedding as $h_u = \theta_u$ and set $\phi_u = \emptyset$, where \emptyset denotes nonexistence. Possible decoders include: $\sigma(h_u^\top h_v)$, $\text{MLP}(h_u \odot h_v)$, $\text{MLP}(h_u \| h_v)$.

For complex-valued encoder, we define the complex-valued embedding as $z_u = \theta_u \odot \exp(i\phi_u)$, where i is the imaginary unit. Possible decoders include: $\text{Direc}(z_u, z_v)$, $\text{MLP}(\theta_u \| \theta_v \| \phi_u \| \phi_v)$. Here, $\text{Direc}(\cdot)$ refers to the direction-aware decoder defined in DUPLEX (Ke et al., 2024).

For gravity-inspired encoder, we define the real-valued embedding as $h_u = \theta_u$ and set the mass parameter $m_u = g(\phi_u)$, where $g(\cdot)$ is a function or neural network that converts ϕ_u into a scalar (Zhou et al., 2022). Possible decoders include: $\sigma(m_v - \lambda \log \|h_u - h_v\|_2^2)$ (Salha et al., 2019), $\sigma(m_v - \lambda \log(\text{dist}_{\mathbb{D}_c^{d'}}(h_u, h_v)))$ (Zhou et al., 2022). Here, λ is a hyperparameter and $\text{dist}_{\mathbb{D}_c^{d'}}(\cdot)$ represents the hyperbolic distance.

E. Issues with Existing Experimental Setup

E.1. Details of multiple subtask setup

The multiple subtask setup (Zhang et al., 2021; He et al., 2023; Ke et al., 2024) involves four subtasks where graph edges are categorized into four types: positive (original direction), reverse (inverse direction), bidirectional (both directions), and nonexistent (no connection). Each subtask focuses on predicting a specific edge type. The details are as follows:

- Existence Prediction (EP): The model predicts whether a directed edge (u, v) exists in the graph. Both reverse and nonexistent edges are treated as nonexistence.
- Directed Prediction (DP): The model predicts the direction of edges for node pairs (u, v) , where either $(u, v) \in E$ or $(v, u) \in E$.
- Three-Type Classification (3C): The model classifies an edge as positive, reverse, or nonexistent.
- Four-Type Classification (4C): The model classifies edges into four categories: positive, reverse, bidirectional, or nonexistent.

Table 7. The results of MagNet (Zhang et al., 2021) as reported in the original paper, alongside the reproduced MagNet and MLP results.

Task	Method	Cornell	Texas	Wisconsin	Cora-ML	CiteSeer
DP	MagNet (reported)	82.9 \pm 3.5	80.9 \pm 4.2	83.3 \pm 3.0	86.5 \pm 0.7	84.8 \pm 1.2
	MagNet (reproduced)	84.69 \pm 2.86	87.15 \pm 4.49	85.72 \pm 4.24	88.56\pm0.44	89.72\pm1.06
	MLP	84.95\pm3.10	89.79\pm4.06	87.21\pm2.48	86.56 \pm 0.70	88.92 \pm 0.56
EP	MagNet (reported)	81.1\pm3.3	83.6 \pm 2.7	82.8\pm2.2	82.7\pm0.7	79.9 \pm 0.6
	MagNet (reproduced)	75.42 \pm 6.25	84.52\pm4.12	78.16 \pm 3.83	80.04 \pm 0.89	83.95 \pm 0.35
	MLP	76.01 \pm 4.64	82.97 \pm 4.33	79.79 \pm 2.71	79.47 \pm 1.08	84.78\pm0.56

Table 8. The results of MLP and baselines under PyGSD (He et al., 2023) setup on Direction Prediction (DP) task.

Method	Cora-ML	CiteSeer	Telegram	Cornell	Texas	Wisconsin
MLP	86.13 \pm 0.45	85.51 \pm 0.63	95.61 \pm 0.15	86.40\pm2.60	83.08\pm4.33	87.95\pm2.65
DGCN	85.49 \pm 0.75	84.85 \pm 0.56	96.03 \pm 0.35	84.55 \pm 3.71	79.59 \pm 5.09	84.57 \pm 3.59
DiGCN	85.37 \pm 0.54	83.88 \pm 0.82	94.95 \pm 0.54	85.41 \pm 2.78	76.57 \pm 3.98	82.41 \pm 2.56
DiGCNIB	86.12 \pm 0.42	85.58 \pm 0.56	95.99 \pm 0.44	86.28 \pm 3.37	82.27 \pm 3.51	87.07 \pm 2.16
MagNet	86.33\pm0.54	85.80\pm0.63	96.97\pm0.21	83.29 \pm 4.28	80.25 \pm 4.78	86.60 \pm 2.72

Table 9. The results of MLP and baselines under PyGSD (He et al., 2023) setup on Existence Prediction (EP) task.

Method	Cora-ML	CiteSeer	Telegram	Cornell	Texas	Wisconsin
MLP	78.85\pm0.83	71.03 \pm 0.89	82.72 \pm 0.57	68.41 \pm 2.05	69.58\pm2.29	72.53\pm2.27
DGCN	76.45 \pm 0.49	70.72 \pm 0.79	83.18 \pm 1.55	67.95 \pm 2.27	63.65 \pm 2.40	68.12 \pm 2.86
DiGCN	76.17 \pm 0.49	72.00 \pm 0.88	83.12 \pm 0.43	67.16 \pm 1.82	63.54 \pm 3.85	67.01 \pm 2.47
DiGCNIB	78.80 \pm 0.51	74.55\pm0.91	84.49 \pm 0.51	69.77\pm2.05	67.60 \pm 3.44	70.78 \pm 2.79
MagNet	77.37 \pm 0.45	71.47 \pm 0.71	85.82\pm0.39	68.98 \pm 2.27	65.94 \pm 1.88	71.23 \pm 2.53

E.2. Details of experimental setting and more results

Experimental setting. In this part of the experiment, we strictly follow the configurations of each setup and reproduce the results using the provided codes. For the MLP model, we implement a simple two-layer network with 64 hidden units, while the learning rate and weight decay are tuned according to the settings of each setup to ensure a fair comparison. For the MagNet (Zhang et al., 2021) setup, we reproduce the reported MagNet results and include the MLP results. For PyGSD (He

et al., 2023) setup, we get the results in our environment using their baseline code and settings, and report the MLP results. For DUPLEX (Ke et al., 2024), we reproduce the DUPLEX results and additionally report the results of graph propagation without using the test edges and the MLP results.

Table 10. Link prediction results for CiteSeer dataset under the DUPLEX (Ke et al., 2024) setup: no superscripts are from the DUPLEX paper, [†] indicates reproduction with test set edges in training, and [‡] indicates reproduction without test set edges in training.

Method	EP(ACC)	EP(AUC)	DP(ACC)	DP(AUC)	3C(ACC)	4C(ACC)
MagNet	80.7±0.8	88.3±0.4	91.7±0.9	96.4±0.6	72.0±0.9	69.3±0.4
DUPLEX	95.7±0.5	98.6±0.4	98.7±0.4	99.7±0.2	94.8±0.2	91.1±1.0
DUPLEX [†]	92.11±0.78	95.85±0.87	97.54±0.54	98.93±0.59	88.22±1.06	84.77±1.01
MLP [†]	85.74±1.80	93.33±1.27	97.55±0.97	99.58±0.52	81.20±0.82	76.30±0.62
DUPLEX [‡]	83.59±1.47	89.34±1.03	85.56±1.36	91.82±0.98	76.37±2.07	73.80±2.01
MLP [‡]	77.34±1.86	87.36±1.26	89.19±0.95	95.97±0.61	67.82±1.21	64.25±1.35

Results with the MagNet setup. Table 7 presents the results of MagNet (Zhang et al., 2021) as reported in the original paper, alongside the reproduced MagNet and MLP results, with the highest values bolded for emphasis. These results directly correspond to Figures 1(a) and 1(b).

Results with the PyGSD setup. PyGSD (He et al., 2023) is a software package for Signed and Directed Graphs, built on PyTorch Geometric (PyG) (Fey & Lenssen, 2019). Tables 8 and 9 present the results of MLP alongside several baselines on the Direction Prediction (DP) and Existence Prediction (EP) tasks, with the highest values highlighted in bold. The baselines include DGCN (Tong et al., 2020b), DiGCN (Tong et al., 2020a), DiGCNIB (Tong et al., 2020a), and MagNet (Zhang et al., 2021), as used in PyGSD. Across six datasets, MLP demonstrates competitive performance, achieving state-of-the-art results for both tasks on the Texas and Wisconsin datasets.

Results with the DUPLEX setup. In Table 10, we present the link prediction results for the CiteSeer dataset under the DUPLEX setup. These results, consistent with those in Table 3, highlight two key observations: (1) MLP outperforms DUPLEX on several tasks, and (2) label leakage in DUPLEX significantly impacts the results. Additionally, Figure 7 illustrates the number of samples and the accuracy for each class in the DUPLEX setup on the CiteSeer dataset for the 4C task. These findings, consistent with those in Figure 1(c), further emphasize the class imbalance issue in the 4C task.

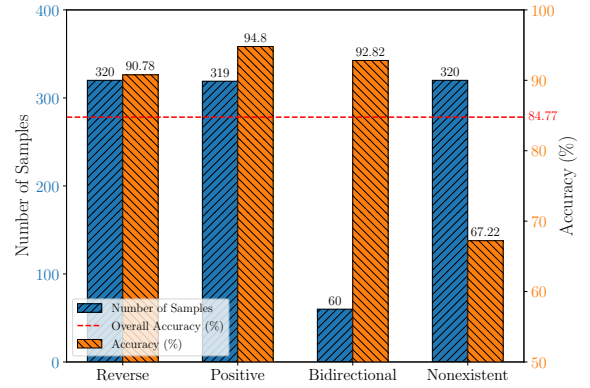


Figure 7. The number of samples and accuracy for each class of DUPLEX on the CiteSeer dataset in the 4C task.

F. Details and Experimental Setting for SDGAE

F.1. More details of graph convolution

The graph convolutional layer of SDGAE is defined as:

$$\begin{bmatrix} \mathbf{S}^{(\ell+1)} \\ \mathbf{T}^{(\ell+1)} \end{bmatrix} = \begin{bmatrix} w_S^{(\ell)} \\ w_T^{(\ell)} \end{bmatrix} \odot \begin{bmatrix} \mathbf{0} & \tilde{\mathbf{A}} \\ \tilde{\mathbf{A}}^\top & \mathbf{0} \end{bmatrix} \begin{bmatrix} \mathbf{S}^{(\ell)} \\ \mathbf{T}^{(\ell)} \end{bmatrix} + \begin{bmatrix} \mathbf{S}^{(\ell)} \\ \mathbf{T}^{(\ell)} \end{bmatrix}. \quad (20)$$

Expanding this formulation, the source and target embeddings at each layer are denoted as:

$$\mathbf{S}^{(\ell+1)} = w_S^{(\ell)} \tilde{\mathbf{A}} \mathbf{T}^{(\ell)} + \mathbf{S}^{(\ell)}, \quad \mathbf{T}^{(\ell+1)} = w_T^{(\ell)} \tilde{\mathbf{A}}^\top \mathbf{S}^{(\ell)} + \mathbf{T}^{(\ell)}. \quad (21)$$

If we denote $\mathbf{X}_S = \mathbf{S}^{(0)} = \text{MLP}_S(\mathbf{X})$ and $\mathbf{X}_T = \mathbf{T}^{(0)} = \text{MLP}_T(\mathbf{X})$, we can derive:

$$\begin{aligned}\mathbf{S}^{(1)} &= w_S^{(0)} \tilde{\mathbf{A}} \mathbf{X}_T + \mathbf{X}_S, \\ \mathbf{T}^{(1)} &= w_T^{(0)} \tilde{\mathbf{A}}^\top \mathbf{X}_S + \mathbf{X}_T, \\ \mathbf{S}^{(2)} &= \mathbf{X}_S + \left(w_S^{(1)} + w_S^{(0)}\right) \tilde{\mathbf{A}} \mathbf{X}_T + w_S^{(1)} w_T^{(0)} \tilde{\mathbf{A}} \tilde{\mathbf{A}}^\top \mathbf{X}_S, \\ \mathbf{T}^{(2)} &= \mathbf{X}_T + \left(w_T^{(1)} + w_T^{(0)}\right) \tilde{\mathbf{A}}^\top \mathbf{X}_S + w_T^{(1)} w_S^{(0)} \tilde{\mathbf{A}}^\top \tilde{\mathbf{A}} \mathbf{X}_T.\end{aligned}$$

These results represent the source and target embeddings for layers $L = 1, 2$. The propagation pattern closely resembles that of spectral-based GNNs (Chien et al., 2021; He et al., 2021; 2022). Specifically, the propagation in spectral-based GNNs is expressed as $\mathbf{Y} = \sum_{\ell=0}^L w_\ell \tilde{\mathbf{A}}^\ell$, where w_ℓ denotes the learnable polynomial weights and $\tilde{\mathbf{A}}$ represents the symmetrically normalized adjacency matrix of an undirected graph. By comparison, SDGAE achieves spectral-based propagation by learning separate weights w_S and w_T . Further spectrum analysis of SDGAE will be explored in future research.

Time Complexity. The primary time complexity of SDGAE arises from the graph convolution process. Based on Equation (21), the time complexity of SDGAE’s convolution is given by $O(2Lmd)$, where m is the number of edges, L is the number of layers, and d is the embedding dimension. This complexity scales linearly with m and is lower than that of DiGAE, which involves multiple learnable weight matrices.

F.2. Experimental setting

For the SDGAE experimental setting, we aligned our settings with those of other baselines in DirLinkBench to ensure fairness. For the MLP used in \mathbf{X} initialization, we set the number of layers to one or two, matching DiGAE’s convolutional layer configurations. The number of hidden units and the embedding dimension were both set to 64. The learning rate (lr) was chosen as either 0.01 or 0.005, and weight decay (wd) was set to 0.0 or 5e-4, following the configurations of most GNN baselines. The number of convolutional layers L was set to 3, 4, or 5. We performed a grid search to optimize parameters on the validation set, and Table 11 presents the corresponding SDGAE parameters for different datasets.

Table 11. The parameters of SDGAE on different datasets.

Datasets	hidden	embedding	MLP layer	L	lr	wd
Cora-ML	64	64	1	5	0.01	0.0
CiteSeer	64	64	1	5	0.01	0.0
Photo	64	64	2	5	0.005	0.0
Computers	64	64	2	3	0.005	0.0
WikiCS	64	64	2	5	0.005	5e-4
Slashdot	64	64	2	5	0.01	5e-4
Epinions	64	64	2	5	0.005	0.0

G. More Details of DirLinkBench

G.1. Datasets and baselines

Datasets Details. Table 12 summarizes the statistical characteristics of seven directed graphs. Avg. Degree indicates average node connectivity and %Directed Edges reflects inherent directionality. Detailed descriptions:

- Cora-ML (McCallum et al., 2000; Bojchevski & Günnemann, 2018) and CiteSeer (Sen et al., 2008) are two citation networks. Nodes represent academic papers, and edges represent directed citation relationships.
- Photo and Computers (Shchur et al., 2018) are two Amazon co-purchasing networks. Nodes denote products, and directed edges denote the sequential purchase relationships.
- WikiCS (Mernyei & Cangea, 2020) is a weblink network where nodes represent computer science articles from Wikipedia and directed edges correspond to hyperlinks between articles.
- Slashdot (Ordozgoiti et al., 2020) and Epinions (Massa & Avesani, 2005) are two social networks, where nodes represent users. Edges in Slashdot indicate directed social interactions between users, and edges in Epinions represent unidirectional trust relationships between users.

Table 12. Statistics of DirLinkBench datasets.

Datasets	#Nodes	#Edges	Avg. Degree	#Features	%Directed Edges	Description
Cora-ML	2,810	8,229	5.9	2,879	93.97	citation network
CiteSeer	2,110	3,705	3.5	3,703	98.00	citation network
Photo	7,487	143,590	38.4	745	65.81	co-purchasing network
Computers	13,381	287,076	42.9	767	71.23	co-purchasing network
WikiCS	11,311	290,447	51.3	300	48.43	weblink network
Slashdot	74,444	424,557	11.4	-	80.17	social network
Epinions	100,751	708,715	14.1	-	65.04	social network

Baseline Implementations. For MLP, GCN, GAT, and APPNP, we use the PyTorch Geometric (PyG) library (Fey & Lenssen, 2019) implementations. For DCN, DiGCN, and DiGCNIB, we rely on the PyTorch Geometric Signed Directed (PyGSD) library (He et al., 2023) implementations. For other baselines, we use the original code released by the authors. Here are the links to each repository.

- Pytorch Geometric library: https://github.com/pyg-team/pytorch_geometric/tree/master/benchmark
- PyTorch Geometric Signed Directed library: https://github.com/SherylHYX/pytorch_geometric_signed_directed
- STRAP: <https://github.com/yinyuan1227/STRAP-git>
- ODIN: <https://github.com/hsyoo32/odin>
- ELTRA: <https://github.com/mrhhyu/ELTRA>
- DiGAE: <https://github.com/gidiko/DiGAE>
- DHYPR: <https://github.com/hongluzhou/dhypr>
- DirGNN: <https://github.com/emalgorithm/directed-graph-neural-network>
- MagNet: <https://github.com/matthew-hirn/magnet>
- DUPLEX: <https://github.com/alipay/DUPLEX>

Baseline setting. For STRAP, ODIN, and ELTRA, we use four decoders for selection: $\sigma(s_u^\top t_v)$, $\text{LR}(s_u \odot t_v)$, $\text{LR}(s_u \| t_v)$, and $\text{LR}(s_u \| s_v \| t_u \| t_v)$ (Yoo et al., 2023). For embedding generation, we follow the parameter settings specified in their respective papers and refer to the code for further details. For MLP, GCN, GAT, APPNP, DGCN, DiGCN, DiGCNIB, and DirGNN, we use four combinations of loss functions and decoders for selection: CE loss with $\text{MLP}(h_u \| h_v)$, BCE loss with $\text{MLP}(h_u \| h_v)$, BCE loss with $\text{MLP}(h_u \odot h_v)$, and BCE loss with $\sigma(h_u^\top h_v)$. For MagNet, DUPLEX, DHYPR, and DiGAE, we follow the reported loss function and decoder settings from their respective papers. For all GNNs, we set the number of epochs to 2000 with an early stopping criterion of 200 and run each experiment 10 times to report the mean and standard deviation differences. The hyperparameter settings for the baselines are detailed below, where 'hidden' represents the number of hidden units, 'embedding' refers to the embedding dimension, 'undirected' indicates whether an undirected training graph is used, 'lr' stands for the learning rate, and 'wd' denotes weight decay.

- MLP: hidden: 64, embedding: 64, layer: 2, lr: {0.01, 0.005}, wd: {0.0, 5e-4}.
- GCN: hidden: 64, embedding: 64, layer: 2, undirected: {True, False}, lr: {0.01, 0.005}, wd: {0.0, 5e-4}.
- GAT: hidden: 8, heads: 8, embedding: 64, layer: 2, undirected: {True, False}, lr: {0.01, 0.005}, wd: {0.0, 5e-4}
- APPNP: hidden: 64, embedding: 64, K : 10, α : {0.1, 0.2}, undirected: {True, False}, lr: {0.01, 0.005}, wd: {0.0, 5e-4}.
- DGCN: hidden: 64, embedding: 64, lr: {0.01, 0.005}, wd: {0.0, 5e-4}.
- DiGCN and DiGCNIB: hidden: 64, embedding: 64, α : {0.1, 0.2}, layer: 2, lr: {0.01, 0.005}, wd: {0.0, 5e-4}.

- DirGNN: hidden: 64, embedding: 64, layer: 2, α : {0.0, 0.5, 1.0}, jk: {'cat', 'max'}, normalize: {True, False}, lr: {0.01, 0.005}, wd: {0.0, 5e-4}.
- MagNet: hidden: 64, embedding: 64, layer: 2, K : {1, 2}, q : {0.05, 0.1, 0.15, 0.2, 0.25}, lr: {0.01, 0.005}, wd: {0.0, 5e-4}.
- DUPLEX: hidden: 64, embedding: 64, layer: 3, head: 1, loss weight: {0.1, 0.3}, loss decay: {0.0, 1e-2, 1e-4}, lr: {0.01, 0.005}, wd: {0.0, 5e-4}.
- DHYPR: hidden: 64, embedding: 32, proximity: {1, 2}, λ : {0.01, 0.05, 1, 5}, lr: {0.01, 0.001}, wd: {0.0, 0.001}.
- DiGAE: hidden: 64, embedding: 64, single layer: {True, False}, (α, β) : {0.0, 0.2, 0.4, 0.6, 0.8}², lr: {0.01, 0.005}, wd: {0.0, 5e-4}.

G.2. Metric description

Mean Reciprocal Rank (MRR) evaluates the capability of models to rank the first correct entity in link prediction tasks. It assigns higher weights to top-ranked predictions by computing the average reciprocal rank of the first correct answer across queries: $MRR = \frac{1}{|Q|} \sum_{i=1}^{|Q|} \frac{1}{rank_i}$, where $|Q|$ is the total number of queries and $rank_i$ denotes the position of the first correct answer for the i -th query. MRR emphasizes early-ranking performance, making it sensitive to improvements in top predictions.

Hits@K measures the proportion of relevant items that appear in the top-K positions of the ranked list of items. For N queries, $Hits@K = \frac{1}{N} \sum_{i=1}^N \mathbf{1}(rank_i \leq K)$, where $rank_i$ is the rank of the i -th sample and the indicator function $\mathbf{1}$ is 1 if $rank_i \leq K$, and 0 otherwise. Following the OGB benchmark (Hu et al., 2020), link prediction implementations compare each positive sample’s score against a set of negative sample scores. A "hit" occurs if the positive sample’s score surpasses at least K-1 negative scores, with final results averaged across all queries.

Area Under the Curve (AUC) measures the likelihood that a positive sample is ranked higher than a random negative sample. $AUC = \frac{\sum_{i=1}^M \sum_{j=1}^N \mathbf{1}(s_i^{pos} > s_j^{neg})}{M \times N}$, where M and N are positive/negative sample counts, s_i^{pos} and s_j^{neg} their prediction scores. Values approaching 1 indicate perfect separation of positive and negative edges.

Average Precision (AP) is defined as the area under the Precision-Recall (PR) curve. Formally, $AP = \sum_{i=1}^N (R_i - R_{i-1}) \times P_i$, where P_i is the precision at the i -th threshold, R_i is the recall at the i -th threshold, and N is the number of thresholds considered.

Accuracy (ACC) measures the proportion of correctly predicted samples among all predictions. Formally, $ACC = \frac{TP+TN}{TP+TN+FP+FN}$, where TP , TN , FP , and FN represent true positives, true negatives, false positives, and false negatives, respectively.

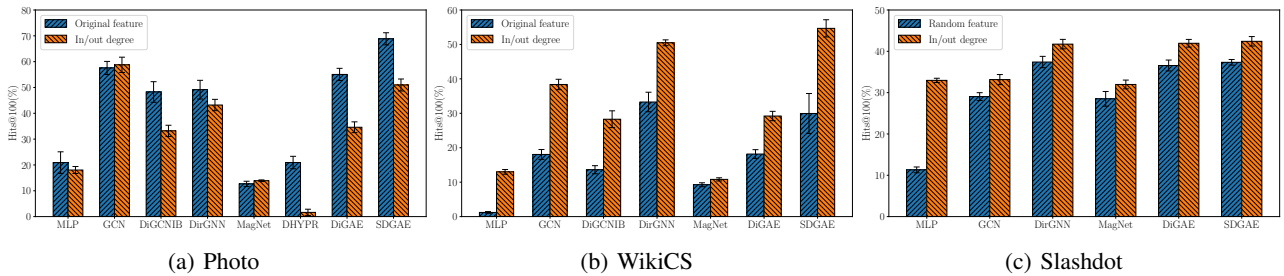


Figure 8. Comparison of various methods’ performance using original features, in/out degrees, or random features as inputs on 3 datasets.

G.3. Additional results in analysis

G.3.1. FETURE INPUTS

In Figures 8(a) and 8(b), we compare the performance of various methods using original features and in/out degrees as inputs on Photo and WikiCS. Figure 8(c) presents a similar comparison using random features and in/out degrees as inputs on Slashdot. The results highlight the significant impact of feature inputs on GNN performance and also demonstrate that in-/out-degree information plays a crucial role in link prediction.

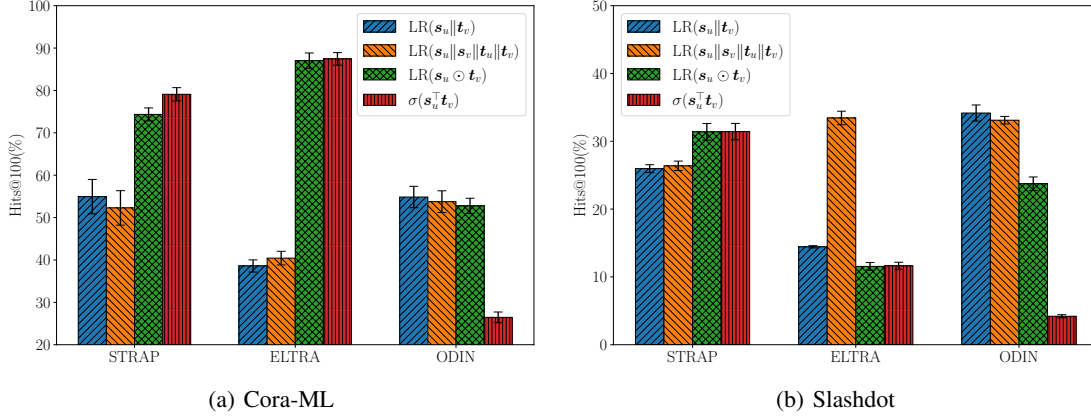


Figure 9. Comparison of different decoders on embedding methods

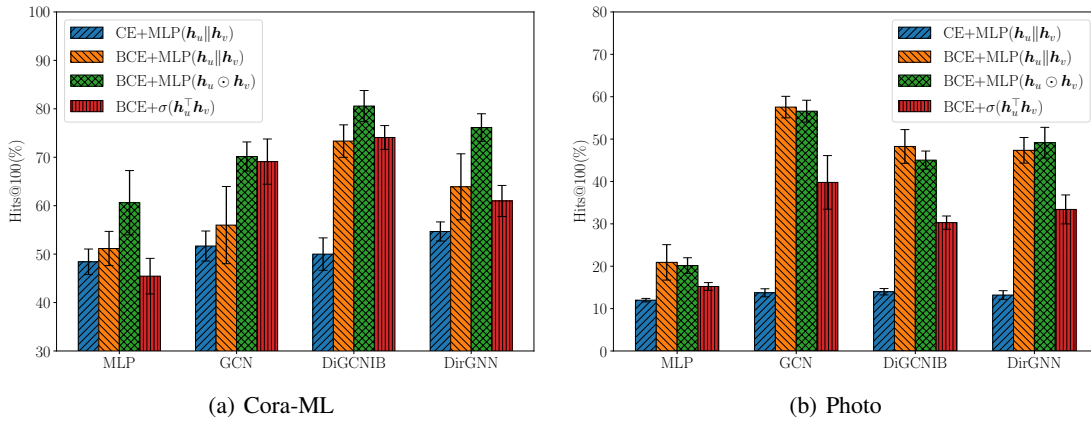


Figure 10. Comparison of various loss functions with different decoders on GNNs.

G.3.2. LOSS FUNCTION AND DECODER

We present a comparison of different decoders on embedding methods in Figure 9 and a comparison of various loss functions with different decoders on GNNs in Figure 10. These results highlight the significant impact of the loss function and decoder on the performance of directed link prediction methods. For embedding methods, even when using the same embeddings, different decoders can lead to substantial variations in performance. Notably, on the Slashdot dataset, ELTRA and ODIN are particularly sensitive to decoder settings. Furthermore, the results from GNNs on Cora-ML and Photo demonstrate that BCE loss provides a clear advantage. These findings emphasize the importance of carefully selecting loss functions and decoder configurations in link prediction tasks.

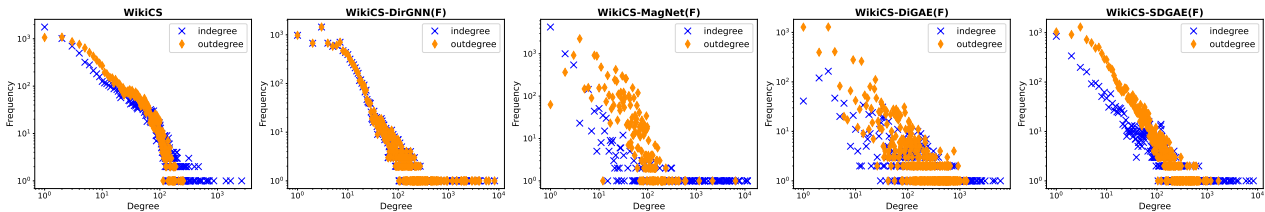


Figure 11. Degree distribution of WikiCS graph and its reconstruction graph generated by GNNs using the original feature as inputs.

G.3.3. DEGREE DISTRIBUTION

We present the degree distribution of the WikiCS graph alongside its reconstructed versions generated by ELTRA and GNNs in Figures 11 and 12. The GNNs use either the original features or the in/out degrees as inputs. First, we observe

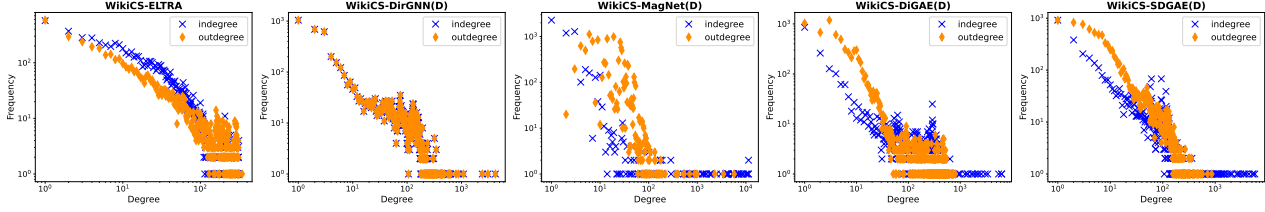


Figure 12. Degree distribution of WikiCS’s reconstruction graph generated by ELTRA and GNNs using the in/out degrees as inputs.

that ELTRA does not effectively preserve the degree distribution of WikiCS. This may be because ELTRA is primarily designed for directed graphs with many directed edges (Hamedani et al., 2023), whereas WikiCS contains many undirected edges, which likely contributes to its poor performance on this dataset. Second, when GNNs use in/out degrees as inputs, they better preserve the degree distribution, which explains their improved performance on WikiCS for the link prediction task. This finding further underscores the importance of degree distribution in link prediction. Finally, comparing DiGAE and SDGAE, we find that SDGAE preserves the degree distribution more effectively, demonstrating the advantages of our proposed SDGAE.

Table 13. The impact of normalization of adjacency matrix on DiGAE and SDGAE.

Methods	Cora-ML	CiteSeer	Photo	Computers
DiGAE ($\hat{D}_{out}^{-\beta} \hat{A} \hat{D}_{in}^{-\alpha}$)	82.06±2.51	83.64±3.21	55.05±2.36	41.55±1.62
DiGAE ($\hat{D}_{out}^{-1/2} \hat{A} \hat{D}_{in}^{-1/2}$)	70.89±3.59	71.60±6.21	38.75±5.20	32.73±5.28
SDGAE ($\hat{D}_{out}^{-1/2} \hat{A} \hat{D}_{in}^{-1/2}$)	90.37±1.33	93.69±3.68	68.84±2.35	53.79±1.56

G.3.4. SDGAE VERSUS DiGAE

In Table 13, we compare the impact of different normalizations of the adjacency matrix on DiGAE and SDGAE. Here, $\hat{D}_{out}^{-\beta} \hat{A} \hat{D}_{in}^{-\alpha}$ represents the original settings in the DiGAE paper (Kollias et al., 2022). We searched for the optimal parameters within the given range, $(\alpha, \beta) \in \{0.0, 0.2, 0.4, 0.6, 0.8\}^2$, noting that this does not include $\hat{D}_{out}^{-1/2} \hat{A} \hat{D}_{in}^{-1/2}$. As shown in Table 13, even when DiGAE uses $\hat{D}_{out}^{-1/2} \hat{A} \hat{D}_{in}^{-1/2}$, its performance did not improve. This indicates that SDGAE’s performance gains are not solely due to changes in the normalization of the adjacency matrix.

Table 14. Comparison of negative sampling strategy on Cora-ML and CiteSeer datasets.

Dataset	Sample	MLP	GCN	DiGCNIB	DirGNN	MagNet	DiGAE	SDGAE
Cora-ML	each run	60.61±6.64	70.15±3.01	80.57±3.21	76.13±2.85	56.54±2.95	82.06±2.51	90.37±1.33
	each epoch	34.15±3.54	59.86±9.89	56.74±4.08	49.89±3.59	54.79±2.98	79.76±3.28	89.71±2.36
CiteSeer	each run	70.27±3.40	80.36±3.07	85.32±3.70	76.83±4.24	65.32±3.26	83.64±3.21	93.69±3.68
	each epoch	66.92±6.50	69.48±6.60	61.69±6.87	53.8±12.41	70.56±2.06	87.32±3.79	92.12±3.96

G.3.5. METRIC AND NEGATIVE SAMPLING STRATEGY

We report the DirLinkBench results under the Accuracy metric in Table 15 and compute the average rank and average score for each baseline. From these results, we observe that simple undirected graph GNNs can achieve competitive performance, with only a small gap between different methods. Notably, some methods that perform well under the Hits@100 metric (e.g., STRAP, DiGAE) perform relatively poorly in Accuracy. Additionally, in Appendix H, we provide the complete DirLinkBench results for each metric across the seven datasets, including AUC, AP, and others. Analyzing these results, we find that AUC and AP exhibit minimal differentiation across baselines, making it difficult to accurately assess link prediction effectiveness. This aligns with ongoing discussions regarding the limitations of these metrics for evaluating link prediction tasks on undirected graphs (Yang et al., 2015; Li et al., 2023). Therefore, we argue that ranking-based metrics, such as Hits@K and MRR, are more suitable for link prediction tasks.

We compare the impact of different negative sampling strategies on model performance during training in Table 14,

Table 15. Results of various methods under the **Accuracy** metric (mean \pm standard error%). Results ranked **first**, **second**, and **third** are highlighted. TO indicates methods that did not finish running within 24 hours, and OOM indicates methods that exceeded memory limits.

Method	Cora-ML	CiteSeer	Photo	Computers	WikiCS	Slashdot	Epinions	Avg. Rank \downarrow	Avg. Score \uparrow
STRAP	78.47 \pm 0.77	75.01 \pm 1.40	94.61 \pm 0.10	93.43 \pm 0.07	94.57\pm0.06	88.19 \pm 0.08	91.89 \pm 0.06	8.71	88.02
ODIN	77.16 \pm 0.84	73.63 \pm 1.19	80.60 \pm 0.20	81.73 \pm 0.10	86.39 \pm 0.08	90.39 \pm 0.10	92.42 \pm 0.07	11.86	83.19
ELTRA	85.40 \pm 0.45	80.86 \pm 1.15	91.84 \pm 0.12	89.30 \pm 0.15	85.73 \pm 0.28	88.11 \pm 0.11	90.40 \pm 0.13	9.57	87.38
MLP	81.32 \pm 2.41	74.81 \pm 1.32	88.31 \pm 0.50	85.33 \pm 0.57	84.65 \pm 0.22	89.62 \pm 0.11	92.56 \pm 0.45	11.14	85.23
GCN	82.82 \pm 0.86	79.47 \pm 1.73	95.90\pm0.18	95.69\pm0.13	89.85 \pm 0.35	89.75 \pm 0.17	94.17\pm0.08	5.50	89.66
GAT	88.95\pm0.71	85.94 \pm 1.21	96.17\pm0.20	95.78\pm0.26	88.90 \pm 0.36	88.01 \pm 0.49	92.92 \pm 0.37	4.64	90.95
APPNP	89.90\pm0.73	86.23\pm1.49	94.71 \pm 0.29	94.01 \pm 0.16	87.51 \pm 0.14	90.07 \pm 0.10	94.17\pm0.16	5.07	90.94
DGCN	80.26 \pm 0.69	74.83 \pm 1.46	95.27 \pm 0.94	95.22 \pm 0.20	90.13 \pm 0.37	TO	TO	9.43	87.14
DiGCN	82.47 \pm 0.97	80.38 \pm 1.17	93.86 \pm 0.23	93.44 \pm 0.54	88.89 \pm 0.14	TO	TO	9.86	87.81
DiGCNIB	87.25 \pm 0.58	85.98 \pm 1.19	95.05 \pm 0.27	94.61 \pm 0.31	90.72 \pm 0.10	TO	TO	7.14	90.72
DirGNN	85.83 \pm 0.93	80.34 \pm 1.52	95.34 \pm 0.17	94.68 \pm 0.14	91.55\pm0.25	90.65\pm0.13	93.99 \pm 0.05	4.86	90.34
MagNet	77.51 \pm 0.92	73.73 \pm 1.30	80.16 \pm 0.23	81.43 \pm 0.08	86.59 \pm 0.06	90.45\pm0.09	92.92 \pm 0.05	11.21	83.26
DUPLEX	82.28 \pm 0.93	79.20 \pm 1.79	87.68 \pm 0.52	85.65 \pm 0.27	83.82 \pm 0.23	85.42 \pm 3.42	88.20 \pm 3.86	12.14	84.61
DHYPR	86.04 \pm 0.66	87.33\pm1.39	76.94 \pm 0.63	TO	TO	OOM/TO	OOM/TO	11.71	83.44
DiGAE	86.25 \pm 0.80	81.85 \pm 1.31	91.77 \pm 0.18	89.52 \pm 0.15	82.53 \pm 0.48	85.67 \pm 0.28	90.17 \pm 0.14	9.86	86.82
SDGAE	91.36\pm0.70	91.38\pm0.79	96.16\pm0.14	95.66\pm0.12	92.24\pm0.12	91.05\pm0.20	94.33\pm0.11	1.57	93.17

presenting results for seven GNNs on Cora-ML and CiteSeer. Here, “each run” refers to the default setting in DirLinkBench, where a random negative sample is generated for each run and shared across all models. In contrast, “each epoch” represents a strategy where different models randomly sample negative edges in each training epoch. The positive sample splitting and test set remain consistent across comparisons. These results indicate that modifying the negative sampling strategy during training significantly affects model performance, particularly for single real-valued GNNs, where test performance drops substantially. These findings suggest that negative sampling strategies during training deserve further research. For instance, heuristic-based methods have been proposed as alternatives to random sampling in undirected graphs (Li et al., 2023), which could be explored in future work.

H. Complete Results of DirLinkBench on Seven Datasets

H.1. Results on Cora-ML

Table 16. Benchmark Results on Cora-ML. For all methods, _F indicates the use of original node features as input, while _D indicates the use of in/out degrees as input. Results ranked **first** and **second** are highlighted.

Method	Hits@20	Hits@50	Hits@100	MRR	AUC	AP	ACC
STRAP	67.10±2.55	75.05±1.66	79.09±1.57	30.91±7.48	87.38±0.83	90.46±0.70	78.47±0.77
ODIN	27.10±3.69	40.99±3.10	54.85±2.53	10.75±3.51	85.15±0.84	85.41±0.95	77.16±0.84
ELTRA	70.74±5.47	81.93±2.38	87.45±1.48	19.77±5.22	94.83±0.58	95.37±0.52	85.40±0.45
MLP _F	27.16±6.70	44.28±5.72	60.61±6.64	9.02±3.58	89.93±2.09	88.55±2.51	81.32±2.41
MLP _D	29.84±4.83	44.11±4.73	56.74±2.03	11.84±3.40	86.44±0.74	86.58±0.88	77.95±0.95
GCN _F	37.88±5.60	55.31±4.46	70.15±3.01	14.25±3.49	92.01±1.64	91.45±1.47	82.82±0.86
GCN _D	31.36±3.89	45.03±2.92	58.77±2.96	12.56±2.86	86.12±0.87	86.79±1.01	77.81±0.87
GAT _F	33.42±8.93	58.40±6.55	79.72±3.07	9.30±3.39	94.57±0.45	92.77±0.42	88.95±0.71
GAT _D	30.19±4.23	43.53±2.93	55.09±3.34	11.07±3.68	85.52±1.27	86.19±0.96	77.36±1.13
APNP _F	55.47±4.63	75.16±4.09	86.02±2.88	22.49±6.33	95.94±0.57	95.82±0.59	89.90±0.73
APNP _D	32.21±3.65	45.51±3.76	60.02±3.36	11.89±2.65	88.00±1.08	88.01±1.17	79.28±1.13
DGCN _F	30.86±4.17	41.82±4.43	54.38±4.97	11.01±4.23	85.55±3.40	85.66±2.35	77.82±3.49
DGCN _D	36.30±4.43	50.25±3.42	63.32±2.59	13.98±4.24	87.87±0.96	88.67±0.84	80.26±0.69
DiGCN _F	30.05±5.45	48.87±5.25	63.21±5.72	10.16±4.25	89.48±1.83	89.10±1.99	82.47±0.97
DiGCN _D	34.39±3.69	49.66±4.14	60.10±4.04	12.49±3.83	85.87±1.22	87.13±1.18	77.88±1.01
DiGCNIB _F	45.90±4.97	66.62±3.67	80.57±3.21	17.08±3.90	94.67±0.56	94.21±0.65	87.25±0.58
DiGCNIB _D	37.18±4.60	51.64±3.69	64.72±3.43	12.71±4.08	89.23±0.92	89.36±0.85	81.05±1.05
DirGNN _F	42.48±7.34	59.41±4.00	76.13±2.85	12.01±3.57	93.05±0.87	92.52±0.79	85.83±0.93
DirGNN _D	32.29±2.25	45.53±2.60	58.22±2.50	13.34±5.56	87.06±0.77	87.35±0.80	77.93±1.14
MagNet _F	26.87±3.82	40.58±3.19	53.51±2.00	10.08±3.47	85.21±0.79	85.53±1.00	76.93±0.79
MagNet _D	29.38±3.39	43.28±3.76	56.54±2.95	11.19±3.04	85.23±0.84	86.06±0.94	77.51±0.92
DUPLEX _F	21.73±3.19	34.98±2.37	69.00±2.52	7.74±1.95	88.02±0.95	86.62±1.43	82.28±0.93
DUPLEX _D	17.48±4.69	32.58±8.33	54.50±7.49	5.46±2.10	82.97±4.47	82.97±2.85	75.59±4.87
DHYPR _F	59.81±4.79	77.45±2.56	86.81±1.60	20.56±5.10	96.13±0.28	95.84±0.39	86.04±0.66
DHYPR _D	15.09±4.40	28.96±6.54	42.93±6.63	4.05±1.16	80.83±2.64	79.97±3.02	72.74±3.50
DiGAE _F	56.13±3.80	72.23±2.51	82.06±2.51	20.53±4.21	92.56±0.66	93.70±0.54	86.25±0.80
DiGAE _D	35.40±4.05	49.12±3.44	61.30±2.70	13.71±4.22	86.82±0.85	87.35±0.84	76.01±1.04
SDGAE _F	70.89±3.35	83.63±2.15	90.37±1.33	28.45±5.82	97.24±0.34	97.21±0.17	91.36±0.70
SDGAE _D	35.53±5.41	49.34±4.60	61.40±3.18	14.21±3.71	87.38±1.06	88.19±1.18	78.99±1.34

H.2. Results on CiteSeer

Table 17. Benchmark Results on CiteSeer. For all methods, _F indicates the use of original node features as input, while _D indicates the use of in/out degrees as input. Results ranked **first** and **second** are highlighted.

Model	Hits@20	Hits@50	Hits@100	MRR	AUC	AP	ACC
STRAP	63.28±1.46	67.05±1.32	69.32±1.29	40.70±6.95	81.82±1.44	84.15±0.84	75.01±1.40
ODIN	30.74±3.78	47.91±2.57	63.95±2.98	11.05±2.74	82.22±1.05	81.74±1.10	73.63±1.19
ELTRA	72.34±1.76	79.44±1.54	84.97±1.90	27.87±9.03	90.98±0.86	92.71±0.81	80.86±1.15
MLP _F	35.55±4.39	52.31±4.60	70.27±3.40	16.08±4.88	85.47±1.35	85.16±1.29	74.26±1.64
MLP _D	40.27±4.48	56.27±3.64	68.78±2.21	15.94±3.04	84.09±1.02	84.86±1.12	74.81±1.32
GCN _F	42.27±7.11	62.65±4.22	80.36±3.07	18.28±6.7	89.94±1.04	88.88±1.38	79.47±1.73
GCN _D	43.96±2.35	56.24±3.62	66.15±2.07	19.36±4.96	81.24±1.55	84.33±0.90	73.92±1.43
GAT _F	48.29±6.04	71.86±4.65	85.88±4.98	16.71±5.56	92.90±0.74	91.12±1.53	85.94±1.21
GAT _D	40.29±3.25	55.62±1.92	65.82±2.87	19.00±4.18	82.72±0.67	83.96±0.60	74.18±1.18
APNP _F	59.86±6.54	77.57±5.68	83.57±4.90	20.91±4.39	93.58±0.71	93.09±0.68	86.23±1.49
APNP _D	45.44±3.38	58.18±1.55	68.47±3.00	20.18±5.50	83.48±1.17	85.72±1.00	74.86±1.19
DGCN _F	39.64±6.53	50.85±2.91	62.97±4.79	19.15±4.34	80.60±2.90	81.80±1.85	74.12±2.49
DGCN _D	45.94±3.01	58.38±2.85	68.97±3.39	19.53±4.83	83.38±1.41	85.44±1.01	74.83±1.46
DiGCN _F	38.48±3.50	53.30±5.92	70.95±4.67	15.79±4.05	87.41±2.24	85.02±2.90	80.38±1.17
DiGCN _D	40.65±4.23	52.87±3.85	65.46±3.70	17.39±4.82	83.50±1.12	84.75±0.93	74.65±1.36
DiGCNIB _F	44.90±7.91	69.86±5.13	85.32±3.70	16.61±5.61	92.50±0.57	90.35±1.43	85.98±1.19
DiGCNIB _D	45.68±3.50	58.99±3.92	70.29±2.39	20.22±3.31	85.81±0.69	86.73±0.85	76.54±1.27
DirGNN _F	44.95±7.31	64.00±3.19	76.83±4.24	16.19±4.51	88.44±1.28	88.59±1.14	80.34±1.52
DirGNN _D	40.16±4.84	53.44±3.38	65.62±2.46	16.95±5.45	83.67±1.08	84.59±1.18	73.75±1.31
MagNet _F	32.18±5.04	47.44±3.24	61.55±8.45	12.97±1.73	82.58±1.31	82.70±1.45	73.73±1.30
MagNet _D	39.35±5.13	54.50±3.21	65.32±3.26	15.31±2.45	83.05±1.35	84.14±1.31	73.28±1.21
DUPLEX _F	30.16±5.06	50.90±10.69	73.39±3.42	17.82±4.47	84.63±2.20	83.01±2.10	79.20±1.79
DUPLEX _D	27.98±7.61	50.20±7.36	63.62±3.90	10.95±6.35	80.68±1.15	81.17±1.20	73.75±1.44
DHYPR _F	77.77±4.10	89.35±2.59	92.32±3.72	32.39±10.14	96.61±0.28	96.35±0.50	87.33±1.39
DHYPR _D	24.32±8.59	41.51±6.55	54.27±5.94	6.17±2.12	77.38±1.79	77.35±2.44	70.27±1.35
DiGAE _F	56.12±3.08	71.06±2.49	83.64±3.21	22.88±6.79	91.03±1.14	91.29±1.04	81.85±1.31
DiGAE _D	44.32±1.85	59.91±2.08	69.66±2.11	20.89±4.81	85.28±0.96	86.28±0.96	74.54±0.91
SDGAE _F	81.06±4.50	91.24±2.55	93.69±3.68	42.50±9.76	97.24±0.60	97.13±0.68	91.38±0.79
SDGAE _D	45.03±3.19	57.82±2.00	68.97±1.70	21.41±2.85	85.10±0.98	86.24±0.47	74.83±0.86

H.3. Results on Photo

Table 18. Benchmark Results on Photo. For all methods, _F indicates the use of original node features as input, while _D indicates the use of in/out degrees as input. Results ranked **first** and **second** are highlighted.

Model	Hits@20	Hits@50	Hits@100	MRR	AUC	AP	ACC
STRAP	38.54±5.20	55.21±2.19	69.16±1.44	12.08±3.15	98.54±0.04	98.65±0.05	94.61±0.10
ODIN	5.28±1.36	9.38±1.54	14.13±1.92	1.78±0.66	88.15±0.21	87.34±0.30	80.60±0.20
ELTRA	7.09±1.23	12.86±1.58	20.63±1.93	2.22±0.59	96.89±0.06	95.84±0.13	91.84±0.12
MLP _F	8.83±2.06	14.07±2.87	20.91±4.18	3.18±1.06	95.29±0.37	93.60±1.06	88.31±0.50
MLP _D	7.88±1.56	12.90±0.81	18.04±1.35	2.53±0.40	85.90±0.44	86.44±0.21	77.25±0.51
GCN _F	29.44±3.90	44.12±3.49	57.55±2.54	9.85±2.78	99.04±0.06	98.66±0.10	95.90±0.18
GCN _D	31.47±3.71	44.93±3.34	58.77±2.96	12.56±2.86	86.12±0.87	86.79±1.01	77.71±1.01
GAT _F	25.97±4.22	42.85±4.90	58.06±4.03	8.62±3.07	99.13±0.09	98.93±0.11	96.17±0.20
GAT _D	11.96±1.60	21.83±2.98	31.51±2.16	3.61±0.94	94.41±0.19	94.37±0.19	87.00±0.25
APPNP _F	22.13±2.60	35.30±2.04	47.51±2.51	6.56±1.14	98.54±0.09	98.26±0.12	94.71±0.29
APPNP _D	12.92±1.06	19.42±2.24	26.66±2.14	4.63±1.10	93.29±0.42	92.86±0.40	85.36±0.39
DGCN _F	22.61±4.58	37.09±5.38	51.61±6.33	6.38±1.49	98.74±0.39	98.49±0.45	95.27±0.94
DGCN _D	15.96±3.35	26.88±2.91	35.56±3.52	5.83±1.16	96.26±0.70	95.94±0.76	90.02±1.00
DiGCN _F	18.47±1.89	29.63±2.28	40.17±2.38	6.41±2.41	98.10±0.10	97.69±0.14	93.86±0.23
DiGCN _D	17.00±1.84	25.51±1.39	33.73±1.95	5.71±1.32	95.21±0.19	95.09±0.21	88.29±0.26
DiGCNIB _F	21.42±2.77	34.97±2.67	48.26±3.98	6.82±1.53	98.67±0.14	98.39±0.16	95.05±0.27
DiGCNIB _D	16.00±1.67	24.63±1.84	33.20±2.17	6.11±1.50	96.71±0.07	96.38±0.09	91.30±0.17
DirGNN _F	22.59±2.77	34.65±3.31	49.15±3.62	8.42±2.90	98.76±0.09	98.47±0.13	95.34±0.17
DirGNN _D	21.57±2.11	30.87±2.35	43.21±2.19	8.72±2.08	97.53±0.09	97.26±0.08	92.41±0.20
MagNet _F	5.35±0.50	8.52±0.85	12.66±1.03	1.62±0.39	87.92±0.22	87.19±0.32	80.16±0.23
MagNet _D	5.14±0.54	9.04±0.52	13.89±0.32	1.61±0.31	88.11±0.21	87.48±0.21	80.31±0.14
DUPLEX _F	7.84±1.17	12.64±1.22	17.94±0.66	2.53±0.66	94.22±0.76	93.37±0.91	87.68±0.52
DUPLEX _D	6.97±2.14	9.08±4.95	13.28±6.14	2.26±1.17	87.41±7.05	86.40±5.89	79.73±6.87
DHYPR _F	10.18±1.21	13.66±1.47	20.93±2.41	3.15±0.57	87.35±1.54	88.83±0.95	76.94±0.63
DHYPR _D	0.16±0.14	0.52±0.83	1.63±1.23	0.28±0.06	58.85±1.39	56.65±0.62	53.91±0.66
DiGAE _F	27.79±3.85	43.32±3.36	55.05±2.36	9.38±2.47	97.98±0.08	97.99±0.10	91.77±0.18
DiGAE _D	16.55±1.20	26.17±2.03	34.60±2.09	5.36±1.66	93.14±0.14	93.76±0.11	83.23±0.34
SDGAE _F	40.89±3.86	55.76±4.08	68.84±2.35	14.82±4.22	99.25±0.05	99.16±0.06	96.16±0.14
SDGAE _D	24.76±3.46	38.5±1.66	50.96±2.32	9.16±1.99	98.07±0.15	97.98±0.12	93.57±0.35

H.4. Results on Computers

Table 19. Benchmark Results on Computers. For all methods, _F indicates the use of original node features as input, while _D indicates the use of in/out degrees as input. Results ranked **first** and **second** are highlighted.

Model	Hits@20	Hits@50	Hits@100	MRR	AUC	AP	ACC
STRAP	24.35±3.75	38.14±3.77	51.87±2.07	7.44±1.98	98.19±0.03	98.32±0.03	93.43±0.07
ODIN	4.42±1.18	8.41±1.27	12.98±1.47	1.46±0.63	89.35±0.09	89.15±0.35	81.73±0.10
ELTRA	4.82±0.75	8.66±1.38	14.74±1.55	1.61±0.52	95.63±0.10	95.11±0.14	89.30±0.15
MLP _F	5.51±0.72	9.31±0.90	14.26±0.88	1.63±0.42	92.83±0.36	91.86±0.39	85.33±0.57
MLP _D	6.97±1.22	12.2±0.88	17.57±0.85	2.76±0.75	87.48±0.16	88.69±0.15	78.75±0.36
GCN _F	19.32±2.69	31.47±1.81	43.77±1.75	7.26±1.64	98.97±0.06	98.80±0.06	95.69±0.13
GCN _D	10.59±1.40	17.48±1.07	24.59±1.01	4.33±1.26	94.41±0.10	94.25±0.12	87.00±0.13
GAT _F	14.89±3.24	27.53±2.48	40.74±3.22	3.37±0.92	98.99±0.11	98.76±0.15	95.78±0.26
GAT _D	7.16±1.53	14.49±1.54	21.98±1.04	2.36±0.69	95.20±0.44	94.81±0.47	88.14±0.67
APNP _F	12.40±1.24	21.71±1.13	32.24±1.40	4.86±1.06	98.21±0.08	97.90±0.11	94.01±0.16
APNP _D	9.54±1.53	15.36±1.20	21.92±1.32	3.99±0.83	93.84±0.35	93.49±0.38	85.76±0.52
DGCN _F	17.74±2.16	27.81±1.84	39.92±1.94	6.51±1.53	98.78±0.10	98.59±0.11	95.22±0.20
DGCN _D	11.12±1.50	17.79±1.66	25.20±1.87	4.06±0.70	95.54±0.50	95.30±0.53	88.72±0.74
DiGCN _F	11.68±1.84	19.02±2.06	27.51±1.67	4.61±0.71	97.87±0.24	97.47±0.27	93.44±0.54
DiGCN _D	10.98±1.53	17.76±1.37	24.46±1.51	4.69±1.09	94.86±0.11	94.75±0.12	87.59±0.17
DiGCNIB _F	13.41±2.95	22.54±1.79	32.44±1.85	4.86±0.80	98.46±0.14	98.15±0.17	94.61±0.31
DiGCNIB _D	10.70±0.84	16.69±1.41	24.74±1.41	5.10±1.08	96.50±0.09	96.19±0.11	90.77±0.15
DirGNN _F	13.95±1.66	23.94±1.26	35.65±1.30	5.02±0.60	98.56±0.05	98.28±0.07	94.68±0.14
DirGNN _D	13.09±0.90	21.84±1.54	30.70±0.98	6.14±1.58	96.70±0.08	96.64±0.07	91.08±0.13
MagNet _F	5.02±0.60	8.49±0.48	12.66±0.62	1.74±0.66	89.18±0.08	88.99±0.10	81.43±0.08
MagNet _D	4.50±0.76	8.15±0.89	12.85±0.59	0.97±0.22	89.37±0.03	89.25±0.05	81.61±0.11
DUPLEX _F	7.36±0.85	13.19±0.97	17.90±0.71	2.27±0.63	92.05±0.22	91.45±0.29	85.65±0.27
DUPLEX _D	5.92±1.83	9.04±4.80	14.56±5.51	1.48±0.55	87.00±4.97	86.79±4.33	78.90±5.65
DiGAE _F	19.65±1.33	31.16±1.62	41.55±1.62	5.34±1.18	97.29±0.13	97.12±0.44	89.52±0.15
DiGAE _D	11.94±0.96	19.38±1.60	26.53±1.20	3.58±1.20	92.86±0.28	93.51±0.20	82.11±0.32
SDGAE _F	27.07±2.34	41.37±1.61	53.79±1.56	8.41±1.89	99.07±0.04	99.00±0.03	95.66±0.12
SDGAE _D	15.18±2.22	24.02±1.53	33.51±1.16	5.73±1.33	97.44±0.12	97.32±0.11	92.26±0.24

H.5. Results on WikiCS

Table 20. Benchmark Results on WikiCS. For all methods, _F indicates the use of original node features as input, while _D indicates the use of in/out degrees as input. Results ranked **first** and **second** are highlighted.

Model	Hits@20	Hits@50	Hits@100	MRR	AUC	AP	ACC
STRAP	64.97±1.52	71.10±1.13	76.27±0.92	37.29±9.42	98.66±0.03	98.91±0.02	94.57±0.06
ODIN	3.41±0.60	6.24±0.63	9.83±0.47	1.17±0.35	92.86±0.04	91.90±0.10	86.39±0.08
ELTRA	3.84±0.49	6.62±0.55	9.88±0.70	1.42±0.33	92.66±0.19	92.19±0.23	85.73±0.28
MLP _F	0.24±0.09	0.71±0.40	1.21±0.25	0.15±0.07	71.90±0.54	70.86±0.68	66.26±0.67
MLP _D	4.04±0.72	7.92±0.61	12.99±0.68	1.63±0.20	92.12±0.10	91.90±0.19	84.65±0.22
GCN _F	6.10±1.85	11.25±1.86	18.05±1.43	2.07±0.49	95.86±0.27	95.41±0.45	89.85±0.35
GCN _D	18.15±2.49	30.21±2.51	38.37±1.51	6.09±2.16	95.97±0.08	96.23±0.08	89.58±0.09
GAT _F	1.83±0.54	3.52±2.21	5.60±1.17	0.83±0.31	73.18±3.59	74.81±4.19	54.16±6.34
GAT _D	24.13±4.10	34.32±4.41	40.47±4.10	7.67±2.07	95.72±0.27	96.06±0.33	88.90±0.36
APNP _F	3.71±0.46	6.66±0.76	11.11±1.09	1.64±0.33	92.76±0.63	92.11±0.63	85.56±0.08
APNP _D	7.60±1.75	12.76±3.01	20.23±1.72	2.75±0.70	94.12±0.09	93.89±0.12	87.51±0.14
DGCN _F	5.84±1.79	10.12±3.32	15.88±5.12	2.04±0.50	95.98±0.65	95.45±0.80	89.95±0.96
DGCN _D	8.35±3.46	16.51±2.99	25.91±4.10	2.88±1.11	96.22±0.32	96.04±0.43	90.13±0.37
DiGCN _F	3.63±0.69	6.77±0.98	10.24±0.88	1.58±0.46	92.55±1.53	91.63±1.62	82.60±2.14
DiGCN _D	10.08±1.33	16.32±2.16	25.31±1.84	3.85±0.98	95.59±0.12	95.57±0.12	88.89±0.14
DiGCNIB _F	5.36±0.58	8.28±1.20	13.61±1.18	1.81±0.48	94.00±0.33	93.31±0.39	84.49±1.62
DiGCNIB _D	12.01±2.95	20.99±1.75	28.28±2.44	3.96±1.16	96.36±0.07	96.30±0.08	90.72±0.10
DirGNN _F	11.76±3.31	23.90±3.31	33.28±2.84	4.82±1.77	97.09±0.13	97.04±0.16	91.55±0.25
DirGNN _D	28.16±2.09	40.94±1.19	50.48±0.85	12.08±2.05	97.13±0.09	97.33±0.09	91.28±0.14
MagNet _F	3.41±0.35	6.10±0.45	9.25±0.57	1.42±0.22	92.57±0.08	91.54±0.10	86.06±0.11
MagNet _D	4.13±0.46	6.57±0.34	10.81±0.46	1.26±0.37	93.06±0.06	92.18±0.07	86.59±0.06
DUPLEX _F	2.97±0.52	5.54±0.63	8.52±0.60	0.89±0.22	90.92±0.12	90.06±0.45	83.82±0.23
DUPLEX _D	1.09±0.92	1.53±3.12	5.45±0.19	1.03±0.08	90.93±0.04	90.37±0.23	83.81±0.11
DiGAE _F	7.01±1.78	11.54±1.11	18.17±1.27	2.18±0.78	93.47±1.04	93.20±1.16	76.38±0.21
DiGAE _D	10.6±1.89	19.69±1.98	29.21±1.36	4.59±0.88	93.46±0.22	94.47±0.15	82.53±0.48
SDGAE _F	8.54±3.42	19.60±5.04	29.95±5.80	2.35±0.91	96.64±1.23	96.58±1.20	90.98±1.52
SDGAE _D	33.04±3.27	47.62±1.74	54.67±2.50	11.78±4.11	97.23±0.07	97.58±0.06	92.24±0.12

H.6. Results on Slashdot

Table 21. Benchmark Results on Slashdot. For all methods, _R indicates the use of random node features as input, while _D indicates the use of in/out degrees as input. Results ranked **first** and **second** are highlighted.

Model	Hits@20	Hits@50	Hits@100	MRR	AUC	AP	ACC
STRAP	19.10±1.06	25.39±1.43	31.43±1.21	9.82±1.82	94.74±0.05	95.13±0.05	88.19±0.08
ODIN	14.97±1.40	24.91±1.19	34.17±1.19	4.44±1.59	96.58±0.07	96.75±0.06	90.39±0.10
ELTRA	18.02±2.11	26.31±0.95	33.44±1.00	5.53±1.77	94.65±0.03	95.23±0.04	88.11±0.11
MLP _R	4.25±0.71	7.26±0.74	11.31±0.70	1.28±0.33	72.86±0.37	76.72±0.21	66.16±0.26
MLP _D	14.16±5.22	24.01±0.79	32.97±0.51	4.14±1.71	95.84±0.07	96.21±0.05	89.62±0.11
GCN _R	12.52±1.30	21.03±1.62	29.04±0.95	3.03±0.73	95.58±0.13	95.69±0.13	89.46±0.12
GCN _D	16.28±1.59	24.51±1.63	33.16±1.22	5.54±2.04	95.90±0.07	96.17±0.06	89.75±0.17
GAT _R	14.82±2.70	22.19±2.78	30.16±3.11	5.11±1.53	96.26±0.18	96.45±0.20	87.14±1.03
GAT _D	12.39±1.47	19.54±1.89	26.65±1.98	4.53±0.78	95.01±0.34	95.25±0.45	88.01±0.49
APPNP _R	14.83±1.18	22.75±1.45	31.25±1.14	4.56±1.37	95.36±0.07	95.72±0.06	88.76±0.09
APPNP _D	15.00±5.47	24.34±1.47	33.76±1.05	5.86±2.78	96.21±0.06	96.43±0.05	90.07±0.10
DirGNN _R	18.72±1.93	28.52±1.09	37.41±1.37	6.19±2.04	96.67±0.05	96.89±0.04	90.24±0.12
DirGNN _D	20.55±2.85	31.20±1.18	41.74±1.15	7.52±3.24	96.95±0.05	97.14±0.06	90.65±0.13
MagNet _R	9.16±1.26	19.58±1.37	28.50±1.78	1.98±0.25	96.31±0.06	96.38±0.06	90.04±0.13
MagNet _D	12.55±0.75	22.34±0.42	31.98±1.06	2.83±0.51	96.57±0.09	96.69±0.10	90.45±0.09
DUPLEX _R	5.67±1.85	11.49±3.36	18.42±2.59	1.81±0.83	94.36±3.25	94.48±2.76	85.42±3.42
DUPLEX _D	2.51±0.64	5.95±1.11	9.39±2.71	0.51±0.01	80.57±3.85	86.52±1.50	77.67±2.24
DiGAE _R	18.89±1.71	27.69±1.41	36.57±1.32	5.49±2.96	95.26±0.29	96.13±0.19	84.27±0.26
DiGAE _D	23.68±0.94	33.97±1.06	41.95±0.93	5.54±1.51	94.30±0.29	95.80±0.12	85.67±0.28
SDGAE _R	18.24±2.05	28.47±1.97	37.34±0.68	5.51±1.65	95.96±0.07	96.31±0.03	90.11±0.11
SDGAE _D	23.57±2.11	33.75±1.48	42.42±1.15	8.41±3.80	96.70±0.10	97.06±0.08	91.05±0.20

H.7. Results on Epinions

Table 22. Benchmark Results on Epinions. For all methods, _R indicates the use of random node features as input, while _D indicates the use of in/out degrees as input. Results ranked **first** and **second** are highlighted.

Model	Hits@20	Hits@50	Hits@100	MRR	AUC	AP	ACC
STRAP	44.66±1.68	53.48±0.86	58.99±0.82	21.18±6.31	96.62±0.06	97.60±0.04	91.89±0.06
ODIN	11.85±3.33	25.99±1.79	36.91±0.47	3.22±0.80	97.72±0.03	97.91±0.03	92.42±0.07
ELTRA	16.89±1.27	28.37±1.53	41.63±2.53	5.81±1.10	96.19±0.04	97.47±0.03	90.40±0.13
MLP _R	3.84±0.65	7.02±0.40	10.18±0.67	1.18±0.36	78.44±0.25	80.67±0.14	67.83±1.93
MLP _D	15.84±3.61	34.11±2.04	44.59±1.62	4.35±1.64	97.85±0.08	98.02±0.07	92.56±0.45
GCN _R	18.26±2.56	30.18±1.71	40.64±1.53	4.04±1.10	96.90±0.04	97.54±0.03	92.10±0.24
GCN _D	12.40±7.59	30.79±9.24	46.10±1.37	3.12±0.71	97.83±0.09	98.15±0.05	94.17±0.08
GAT _R	19.65±3.52	31.90±3.56	43.65±4.88	6.04±2.16	98.35±0.11	98.50±0.11	92.05±1.30
GAT _D	18.18±4.11	27.18±3.95	36.76±5.74	7.98±1.92	97.61±0.29	97.81±0.22	92.92±0.37
APNP _R	17.86±2.53	27.89±1.24	39.06±1.26	4.88±4.14	97.70±0.04	97.92±0.02	92.84±0.06
APNP _D	18.46±3.51	30.84±1.84	41.99±1.23	6.41±3.73	98.36±0.06	98.48±0.06	94.17±0.16
DirGNN _R	25.66±3.33	39.28±1.96	50.10±2.06	7.03±2.70	98.25±0.03	98.46±0.03	93.99±0.05
DirGNN _D	21.35±2.89	34.06±2.53	46.01±2.07	6.12±2.54	98.03±0.03	98.26±0.02	93.48±0.06
MagNet _R	6.41±1.57	12.95±1.51	22.12±1.27	1.62±0.35	97.60±0.03	97.69±0.03	92.79±0.05
MagNet _D	7.68±1.00	16.30±2.36	28.01±1.72	2.53±0.57	97.71±0.03	97.86±0.04	92.92±0.05
DUPLEX _R	3.76±1.94	8.38±4.39	16.50±4.34	1.85±0.39	92.11±2.25	93.78±3.69	88.20±3.86
DUPLEX _D	2.43±0.86	6.74±0.45	12.35±2.64	0.46±0.08	90.61±1.76	88.72±3.26	81.82±3.74
DiGAE _R	29.11±3.51	43.25±1.68	53.27±1.17	8.85±2.81	97.11±0.19	97.78±0.11	89.16±0.24
DiGAE _D	22.56±9.23	43.19±2.97	55.14±1.96	5.33±1.78	96.47±0.18	97.37±0.10	90.17±0.14
SDGAE _R	21.88±2.17	35.28±2.35	45.04±2.18	6.54±1.94	98.11±0.03	98.35±0.03	93.83±0.07
SDGAE _D	32.81±2.67	45.61±1.92	55.91±1.77	11.62±2.86	98.43±0.07	98.64±0.04	94.33±0.11